VYSOKÉ UČENÍ TECHNICKÉ V BRNĚ

FAKULTA STROJNÍHO INŽENÝRSTVÍ

FACULTY OF MECHANICAL ENGINEERING

ÚSTAV MECHANIKY TĚLES, MECHATRONIKY A BIOMECHANIKY

INSTITUTE OF SOLID MECHANICS, MECHATRONICS AND BIOMECHANICS

RYCHLÉ SKENOVÁNÍ EPR SPEKTROSKOPIE NA RELEVANTNÍCH RADIKÁLECH K DNP

RAPID SCAN EPR SPECTROSCOPY ON DNP RELEVANT RADICALS

BAKALÁŘSKÁ PRÁCE

BACHELOR'S THESIS

AUTOR PRÁCE   **Tomáš Fargač**

AUTHOR

VEDOUCÍ PRÁCE   **Ing. Antonín Sojka**

SUPERVISOR

BRNO 2021

Assignment Bachelor's Thesis

Institut:	Institute of Solid Mechanics, Mechatronics and Biomechanics
Student:	**Tomáš Fargač**
Degree program:	Applied Sciences in Engineering
Branch:	Mechatronics
Supervisor:	**Ing. Antonín Sojka**
Academic year:	2020/21

As provided for by the Act No. 111/98 Coll. on higher education institutions and the BUT Study and Examination Regulations, the director of the Institute hereby assigns the following topic of Bachelor's Thesis:

Rapid scan EPR spectroscopy on DNP relevant radicals

Brief Description:

This thesis aims to perform Electron Paramagnetic Resonance (EPR) in the Rapid Scan regime on liquid radical samples. EPR spectroscopy is based on the interaction of microwaves (MW) with electron spins placed in a magnet. Rapid scan EPR (RS–EPR) allows detecting relaxation times of spin states, the most critical information for developing new storage devices and quantum computers. In the rapid scan regime, a high–speed sweep through the resonance causes wiggles in the measured spectrum. These wiggles can be processed to reveal information about spin relaxation times. The main task of the student is to perform rapid scan measurements via the High Field EPR spectrometer at CEITEC and study the dependency of signal to noise ratio on MW beam coupling between the EPR bridge with the probe placed in magnet.

Bachelor's Thesis goals:

1. Description of Rapid scan EPR spectroscopy on DNP relevant radicals

2. Calculation of relaxation times via rapid scans on radicals

3. Study of the effect of beam coupling on the rapid scan signal.

Recommended bibliography:

LAGUTA, O. et al., Multi-frequency rapid-scan HFEPR. Journal of Magnetic Resonance. 2018, 296, 138-142.

GOLDSMITH F. Paul. Quasioptical Systems Gaussian Beam Quasioptical Propagation and Applications IEEE Press Series on RF and Microwave Technology. Wiley-IEEE Press, 1997.

GREINBERG O. et al., Very High Frequency (VHF) ESR/EPR, Springer, 2004

WEIL J. and J. BOLTON. Electron Paramagnetic Resonance: Elementary Theory and Practical Applications. New Jersey: John Wiley & Sons, 2007.

NEUGEBAUER P. et al., Ultra-broadband EPR spectroscopy in field and frequency domains. Phys. Chem. Chem. Phys., 2018.

Deadline for submission Bachelor's Thesis is given by the Schedule of the Academic year 2020/21

In Brno,

L. S.

—————————————————————   —————————————————————
prof. Ing. Jindřich Petruška, CSc.   doc. Ing. Jaroslav Katolický, Ph.D.

Director of the Institute   FME dean

Abstrakt

Elektronová paramagnetická resonanční (EPR) spektroskopie je fyzikálně-chemická metoda sloužící pro zkoumání látek s nepárovými elektrony. Zkoumá rozdělení energií spinu nepárového elektronu v magnetickém poli a přechody mezi jednotlivými spinovými stavy vyvolané působením mikrovlnného záření. Tato bakalářská práce je zaměřena na popis EPR spektroskopie, na výpočet relaxačních časů pomocí rychlých skenů radikálů a na vývoj automatického párovacího softwaru pro skládání Gaussovských paprsků. Výsledek této práce je implementace vyvinutého softwaru, vyhodnocení jeho vlivu na kvalitu signálu a následný výpočet relaxačních časů.

Summary

Electron paramagnetic resonance (EPR) spectroscopy is a Physico-chemical method used to investigate substances with unpaired electrons. It investigates the distribution of spin energies of an unpaired electron in a magnetic field and the transitions between individual spin states caused by the action of microwave radiation. This bachelor thesis is focused on the description of EPR spectroscopy, the calculation of relaxation times using the rapid scan method on radicals and the development of automatic coupling software for Gaussian beam coupling. The result of this work is the implementation of the developed software, evaluation of its influence on the signal quality and subsequent calculation of relaxation times.

Klíčová slova

Elektronová paramagnetická rezonanční spektroskopie, rychlé skenování, relaxační čas, párovací systém

Key words

Electron paramagnetic resonance spectroscopy, rapid scan, relaxation time, coupling systém

Bibliographical reference

FARGAČ, Tomáš. *Rapid scan EPR spectroscopy on DNP relevant radicals.* Brno, 2021. Available at: https://www.vutbr.cz/studenti/zav-prace/detail/132428. Bachelor thesis. Brno University of Technology, Faculty of Mechanical Engineering, Institute of solid mechanics, mechatronics and biomechanics. Thesis supervisor: Antonín Sojka.

Acknowledgment

The main acknowledgment belongs to Ing. Antonín Sojka for his supervision, mentoring, active interest and endless support during the whole time. I would like to also thank to all members of the MOTeS group in the CEITEC BUT for their professional and helpful advices and tips. The special thanks belongs to my family who supported me during the whole process.

Declaration

I declare that the bachelor's thesis is my work under the supervision of Ing. Antonín Sojka and that all literature sources are listed in references and quoted completely and correctly.

………..………………………….

Author`s signature

Contents

1. Introduction

Nanotechnology is becoming a hot topic because of its possible applications in broad spectrum of fields such as medicine, mechanical engineering, and electronics. One of the applications are advanced materials. This raises a demand for more detailed understanding of the molecular structure. The electron paramagnetic resonance spectroscopy is a method of studying interactions of paramagnetic radicals with microwaves in a magnetic field.

For performing an EPR experiments the sample needs to be irradiated. Then the absorption of the microwave is recorded. In CEITEC BUT the spectroscope is unique because it consists of two separated parts, the magnet, and the quasi-optical table with five degrees of freedom, which moves above the magnet. This brings a necessity of coupling the table precisely above the probe inserted in magnet. The coupling, while done manually, is highly time consuming. This bachelor's thesis aims to develop the software which couples the table and a magnet automatically.

There are several possibilities how to perform an EPR experiment, one of which is rapid scan. The method when the frequency is quickly swept through the resonance point. This causes wiggles in the recorded signal. These wiggles contain an information about relaxation times of the sample. This thesis will demonstrate the influence of the coupling software on the quality of recorded signal and then, from the enhanced signal, the relaxation time of the examined sample will be computed.2. Introduction to the EPR

2. Introduction to the EPR

2.1 History

The history of electron paramagnetic resonance (EPR) and nuclear paramagnetic resonance (NMR) dates back towards the end of World War II as a consequence of the components developed for Radio Detection And Ranging (RADAR). Yevgeny Konstantinovich Zavoisky employed the newly developed MW techniques in the construction of the first EPR spectrometer [2]. He was the first one to detect EPR phenomena at Kazan University in 1944. He also tried to detect the NMR in solids and liquids before. Even though he had a sufficient enough detection system for the resonance signals he was not able to fulfil strict requirements for a homogenous magnetic field at that time. Two years later in 1946, the NMR in solids and liquids was observed by a group of scientists around Purcell, Torrey and Pound at Harvard and independently by Bloch, Hansen and Packard at Stanford. These NMR experiments were very quickly awarded the Nobel Prize in 1952 [1]. However, Zavoisky's work was ignored by western scientific society mainly due to the Iron Curtain as well as the poor political relationship between world powers.

Ever since NMR studies and experiments took off rapidly and gained huge interest. The potential of EPR was rather unrecognized. The reason is very practical. NMR experiments were easier to perform. The exact answer is in the nucleus and electron mass, where the mass of the nucleus is about three orders of magnitude higher than an electron, which leads to resonance at different frequencies. For electron, resonance is observed at GHz frequencies but for nucleus at MHz range [2], which makes experiments way easier to perform because the technologies such as sources of MHz radiation, detectors, waveguides were more accessible than components for higher frequencies at that time, thus the huge interest in NMR at that point in the history.

Moving forward to the late 1970's Yakov Lebedev was the first who performs high-field EPR experiments employing 148 GHz radiation with a 5 T superconducting magnet to enhance sensitivity and resolution in his study of complex spin states [1] mixture of various interactions such as Zeeman, hyperfine etc. (further in chapter 2), which signal often overlaps at lower frequency bands.

Even until today the imbalance and gap between EPR and NMR may be observed. Although NMR is now well established in science and medicine, EPR is becoming a very hot topic in the last decade most importantly thanks to improvements in other fields of technology and engineering (it was only after the end of the Cold War in the early 1990s when low-noise mm microwave sources, fast switches and detectors became available for unclassified research [1]). Technologies in different fields (microwave, cryomagnetic, data processing, and data acquisition) enable huge improvements, particularly in EPR spectroscopy. At the beginning of the EPR experiments, the continuous wave (CW) microwave technique was a staple approach in the irradiation of the sample. Later it was mainly pulsed microwaves and now we are drawing our attention towards Rapid Scan (RS) method. RS is a revolutionary technique that can improve the signal to noise ratio and significantly decreases the acquisition time [39] (the detailed principle is in chapter 3).

2.2 Motivation

The idea of precise measurements of the spin states relaxation on different radicals is very tempting. Even more, if we would take into consideration the rise of the importance of nanotechnology in fields such as mechanical engineering, electronics and medicine. For example, Moore's law says that the number of transistors in a dense integrated circuit (IC) doubles about every two years. Currently, commercially used silicon transistors are at the size of nanometres. To keep up with this pace in order to produce high-performance integrated circuits which spread widely into almost every sophisticated gadget around us, we need to understand the nanostructure of materials and, most importantly its behaviour approaching sizes very close to the size of molecules or even individual atoms soon. This is just a particular example from the world of electronics, although such knowledge and methods would be applicable in many other fields creating new paths to walk on or enhancing existing methods.

Also implementing new techniques such as a dynamic nuclear polarization (DNP, described in detail in chapter 2) on radicals as Tetramethylpiperidinoxyl (TEMPO) to enhance NMR signal by several magnitudes. This kind of technique could enhance current medical procedures such as magnetic resonance imagining (MRI). Implementation of the DNP method into MRI could easily halve the acquisition time which is currently necessary. On one hand, this could lead to higher accessibility of this modern diagnostic procedure. Although, there is still a long way to come until such applications. As scientists, we have to stay positive and do everything we can to better the future.

2.2 Description of the main goal

The final target of this thesis is to perform measurements of spin states on liquid dynamic nuclear polarizable radicals (TEMPO or lithium phthalocyanine (LiPC)) in RS mode on EPR spectrometer at CEITEC BUT and comparing these results with measurements implementing a newly developed automatic coupling mechanism to enhance the signal to noise (S/N) ratio potentially. The path leading to such measurements will be build up through several sub-steps implementing all aspects of mechatronics, which will be covered in the following chapters. A theoretical part gives insight into EPR spectroscopy, description of the instrumentation, coupling and propagation of Gaussian beams. Then the development of an automatic coupling mechanism involving the design of the new mechanical parts for spectrometer and programming a brand-new coupling algorithm. All this eventually results in measurements of spin states and a final discussion on achieved results and their applications.

3. EPR Theory

In this chapter, there is going to be the theory build up around electron spin, spin excitation and relaxation. That will peak out in explaining the dynamic nuclear polarization method as a tool of enhancing NMR signal by tens or hundreds of magnitude.

3.1 Electron Spin

In the EPR spectroscopy sometimes also known as electron spin resonance (ESR) spectroscopy the main object of studies are unpaired electrons. Subatomic particles such as electrons may be described by 4 quantum numbers: principal (n), azimuthal (l), magnetic (m_l) and spin (s).

The principal quantum number (n) describes the energy level of a shell in which an electron is located and may have the value in a range from 1 to the value of the outermost valence electron of the atom ($n = 1, 2, ...$) [32].

The azimuthal quantum number (l), also known as the orbital or angular quantum number. The azimuthal quantum number is the second of a set of quantum numbers that describe the unique quantum state of an electron [33]. It gives information about the shape and symmetry of the electron orbital. Every shape has assigned its quantum number from the following group: $s = 0, p = 1, = 2, f = 3, g = 4$. The azimuthal number may be within the interval: $l = 0, 1, ..., n - 1$; where the n is a principal quantum number.

The magnetic quantum number (m_l) defines the orientation of the electron orbital in space. It distinguishes the orbitals available within a subshell and is used to calculate the azimuthal component of the orientation of the orbital in space [34]. It must lay in the interval $< -l, +l >$; where the l is the azimuthal quantum number and values are spaced by an integer. It describes which case (which space projection of the orbital) from all the possibilities it does occupy.

Finally, the spin quantum number (m_s) describes the angular momentum of an electron. An electron spins around an axis and has both angular momentum and orbital angular momentum. Because angular momentum is a vector, the spin quantum number has both a magnitude (1/2) and direction (+ or -) [35]. An isolated electron, all alone in space without any outside forces, still has an intrinsic angular momentum called spin $\vec{S}$. Because an electron is charged, the angular motion of this charged particle generates a magnetic field. In other words, the electron due to its charge and angular momentum, acts like a little bar magnet, or magnetic dipole, with a magnetic moment $\overrightarrow{\mu_e}$ [3].

The magnitude of an intrinsic angular momentum spin $\left|\vec{S}\right|$ can be calculated from the following equation 2.1

$$\left|\vec{S}\right| = \hbar \cdot \sqrt{s \cdot (s + 1)} \tag{2.1}$$

Where s is the spin quantum number and $\hbar = 1.054\,571\,817 \cdot 10^{-34}\,J \cdot s$ [31] is reduced Planck's constant ($\hbar = \frac{h}{2\pi}$)

3.2 Electron excitation

In nature, it is very common for everything from the macroscale to microscale to occur and exist at a lower possible energy level. On the macroscale, for instance, the ball rolls down the hill to lower its energy and eventually ends up in a stable position with the lowest mechanical energy. On microscale molecules and atoms have the same tendency to be in a stable state with the lowest possible energy (ground state). However, there are methods on how to induce higher energy states than the ground state.

Excitation of the bounded electron elevates its energy after an energy absorption to a higher energetic but still bounded state. If the elevation in energy would be too high the electron would cease the bound to the atom and the atom would become ionized [5]. For example, let us have the free hydrogen atom with a single electron occupying 1s orbital, (Fig. 2-1 A) after irradiating such atom, the electron may absorb the precise amount/quantum of energy equivalent to the energy difference of both states:

$$\Delta E = h\nu \tag{2.2}$$

Where ΔE is the energy difference between states; ν is the frequency of the absorbed radiation; $h = 6.626\ 069\ 934 \cdot 10^{-34}$ J·s [4] is Planck's constant.


(A) (B)
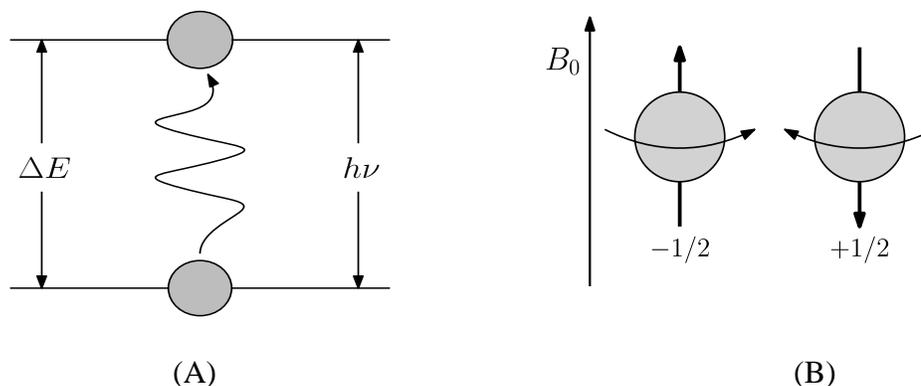
Fig. 2-1   A) Transition associated with the absorption of electromagnetic energy [6]

B) States with minimal and maximal energy level based on the mutual alignment of vectors μ_e and B_0 [3]

An excited state is usually not very stable because a system occurs in a higher energy state than in which it could be, so the electron tends to get back to the ground state to minimalize the overall energy. Very often spontaneous emission (or induced emission if the state is meta-stable) will occur followed by an emission of the energy and again obeying the difference between states according to the equation (2.2). This process is often called decay and it is the opposite of excitation [5].

The process above describes electron excitation in terms of gaining a higher principal quantum number and transitions between different quantum shells (energy levels). Nevertheless, excitation is a lot wider concept. For example, EPR spectroscopy is making use of excitation of spin quantum number. For better understanding such phenomena there is a need to apply the

knowledge described in chapter 2.1 about electron spin, where it is established that electron acts like a little bar magnet, or magnetic dipole, with a magnetic moment $\bar{\mu}_e$ [3]. Without the presence of an outer magnetic field, the unpaired electron may be present at two quantum states +1/2 or -1/2 with the same energy. These states are referred to as degenerated [40]. However, with the outer magnetic field's help, where the electron may be polarized, these two states exhibit a difference in energy levels (Fig. 2-1 B). This is going to be the subject of the following chapter dedicated to the Zeeman effect.

3.3 Zeeman effect

The energy differences studied in EPR spectroscopy are predominately due to the interaction of unpaired electrons in the sample with microwaves and a magnetic field produced in the laboratory. This effect is called the Zeeman Effect. The magnetic field B_0, produces two energy levels for the magnetic moment m_s, of the electron [3].

$$E = \overrightarrow{\mu_e} \cdot \overrightarrow{B_0} \tag{2.3}$$

where the magnetic moment μ_e is:

$$\overrightarrow{\mu_e} = \vec{S} \cdot g \cdot \mu_B \tag{2.4}$$

where the $\vec{S}$ is the intrinsic angular momentum. The parallel alignment has a value of -1/2 and antiparallel +1/2 [3]; $g = 2.002\ 319\ 277\ 8$ [3] (for a free electron) is Landé factor also known as g-factor and $\mu_B = 9.274\ 015\ 4 \cdot 10^{-24}$ J [7] is the exact value of Bohr magneton.

A combination of equations 2.3 and 2.4 gets the electron energy of the magnetic moment:

$$E = \vec{S} \cdot g \cdot \mu_B \cdot \overrightarrow{B_0} \tag{2.5}$$

The two very important assumptions arise from equation 2.5. If the value of an external magnetic field $B_0 = 0$, there is no energy difference between states so $\Delta E = 0$. The second important finding is that the energy difference between the two polarizations has a linear dependency on the magnetic field B_0.
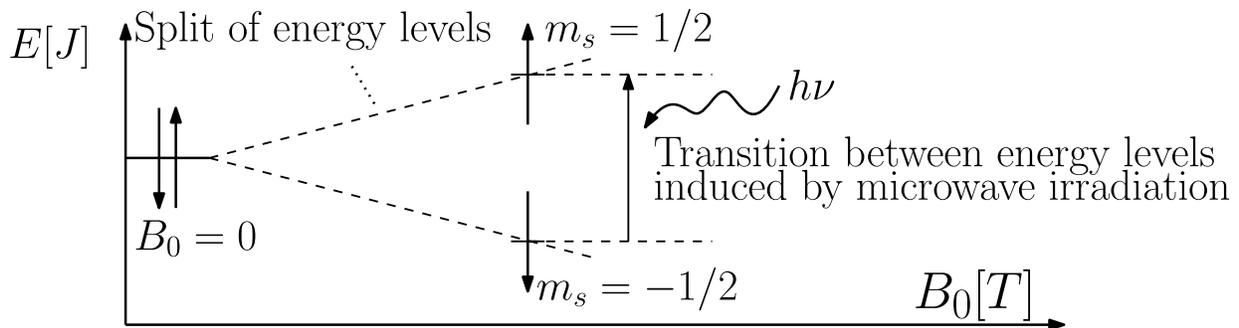

Fig. 2-2   Linear splitting of spectral lines and the increasing energy difference between states in the increasing outer magnetic field B_0 [8]

3.4 The spin Hamiltonian

The Zeeman effect is just an interaction between an electron and a microwave in the magnetic field. Although it may be one of the most significant interactions taking part in the observation of the sample certainly, it is not the only one, especially in spin systems with the spin >1/2 [9]. There is a lot more going on in the sample and several other interactions take part in as well which are splitting the spectral line more and more. In particular, models considering electron-proton interactions and system with higher spins than 1/2.

It is beneficial to quantify all these interactions. In classical mechanics, the system energy can be expressed as the sum of the kinetic and potential energies. For quantum mechanics, the elements of this energy expression are transformed into the corresponding quantum mechanical operators. The Hamiltonian contains the operations associated with the kinetic and potential energies. This may provide a lot more useful information about the composition and arrangement of the studied sample. All these interactions are summed up in the spin Hamiltonian:

$$H = H_{EZ} + H_{ZF} + H_{NZ} + H_{NQ} + H_{EE} + H_{HF} + H_{SHF} \qquad (2.6)$$

Where the individual components are:

H_{EZ} – general Electron-Zeeman interaction between an external magnetic field B_0 and magnetic moment of the electron $\bar{\mu}_e$, the detailed explanation is provided above in chapter 2.3

H_{ZF} – zero-field interaction describes various interactions of the energy levels of an electron spin energy which occurs even without the presence of an external magnetic field at $B_0 = 0$

H_{NZ} – Nuclear-Zeeman is the spin Hamiltonian term describing the interaction of a nuclear spin with the external magnetic field [9]. The interaction very similar to the Electron-Zeeman interaction, however, focused on the energy of the nuclei.

H_{NQ} – The nuclear quadrupole interaction takes place between the electric field gradient with the quadrupole moment of the nuclear charge distribution [10]

H_{EE} – Electron-Electron interaction, since every electron in the sample carries its charge, their magnetic moments naturally interact with each other

H_{HF} – Hyper-Fine interaction between the magnetic moment of the electron $\bar{\mu}_e$ and magnetic moment of its nucleus $\bar{\mu}_n$

H_{SHF} – Super Hyper-Fine interaction between the magnetic moment of the electron $\bar{\mu}_e$ and other nearby nuclei except its own [9]

3.5 Magnetic relaxations

Sub-chapter 2.2 was dedicated to the possibility and the ways of exciting an electron to higher states. However, as stated above, it is either an unstable or meta-stable state thus the relaxation of the electrons occurs after a short time. This phenomenon taking place in the outer magnetic field B_0. Magnetic relaxation describes what is happening shortly after the electron spins are excited into an antiparallel state towards the magnetic field.

Each electron has its magnetic dipole moment (MDM). In a simplified model, the sum of all MDMs is referred to as M_o in the figures showing the average of the system. Before irradiation, all the MDMs are aligned with the magnetic field as shown in Fig. 2-3A(1). In 3D it means that the orientation of M_o slightly precess around the z-axis [11] (amplitude in the z-axis is maximal and projection in the x-y plane is minimal/zero).
After absorbing radiation all the MDMs are flipped from the alignment in the z-direction into the x-y plane [11] (Fig. 2-3A(2)). Immediately after absorbing the microwave pulse the projection of M_o in x-y plane is maximal and amplitude in the z-axis is zero.
During relaxation, the amplitude in the z-axis will slowly increase (Fig. 2-4B) while the amplitude in the x-y plane slowly decreases (Fig. 2-4C). T_1 relaxation is the time taken for the z vector to regain strength, whereas T_2 relaxation is the time taken for the x-y vector to decay. [11]
Important thing is that each return of the electron to the ground state invokes a small but measurable pulse of energy which can be captured and processed. Based on these measurements, characteristic constants T_1 (63% of maxmal strength, Fig. 2-3D) and T_2 (0.37% of maximum, Fig. 2-3E) are determined.
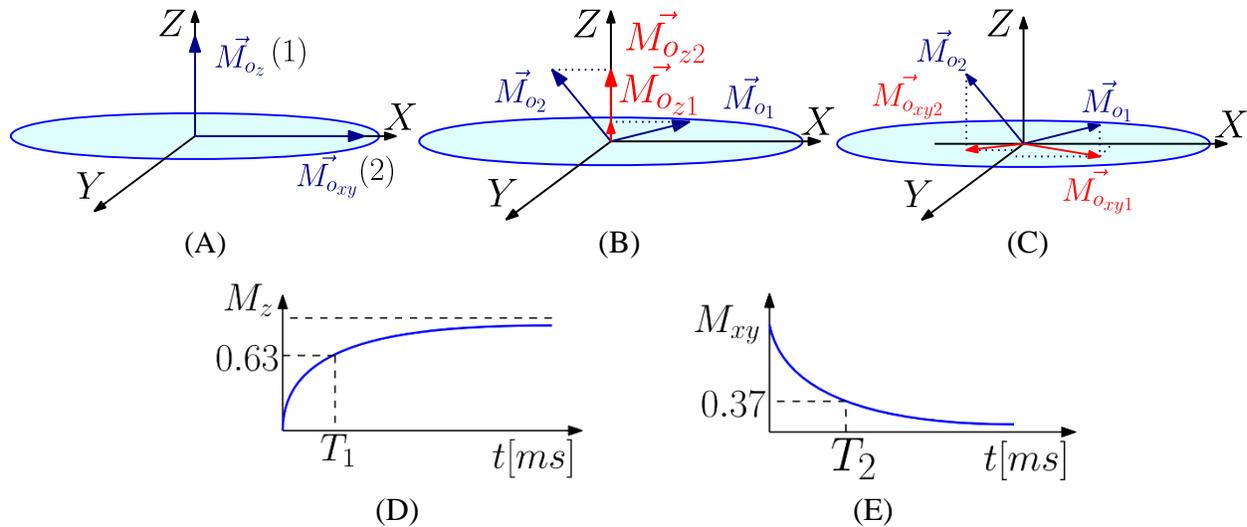

Fig. 2-3   A) System shortly before irradiation, the maximal amplitude of M_o in z-axis (1),
             Immediately after irradiation, maximal projection of M_o in x-y plane (2).
             B) Z-vector of M_o regaining its strength. C) Vanishing x-y projection of M_o.
             D) T_1 relaxation E) T_2 decay

3.6 Dynamic Nuclear Polarization (DNP)

Nowadays the nuclear magnetic resonance is a widely used experimental method. It is also used for example in medicine as MRI, one of the best imagining method currently available. However, it also does have a problematic side. The major problem is low signal intensity. This problem is currently overcome by averaging thousands of images, which takes a large portion of time (tens of minutes to a couple of hours). DNP increases the sensitivity of NMR by transferring the large spin polarization from stable paramagnetic centres to the nuclear spin reservoir [38], which erases the need for averaging all of the images thus lowering the acquisition time down to a single measurement with a duration of tens milliseconds up to a couple of seconds.

The essential benefit is that getting a much larger signal intensity than without DNP. This opens new opportunities when an experiment takes a lot less time to perform because there is no need to spend so much time averaging plenty of results as it would be necessary without using a DNP. And what is even more interesting that with such a technique, it is possible to look at samples that could not be examined in the classical NMR approach.

An awesome application of THz DNP in NMR is the drastic gain in sensitivity (Fig. 2-4) in the study of amyloid fibrils where the TOTAPOL as a biradical polarizing agent was used [38].
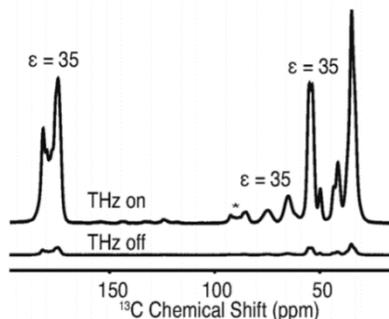

Fig. 2-4   Significantly enhanced signal after application of DNP method and 0.263 THz radiation on the samples of amyloid fibrils by [38]. The figure is taken from [38] and adjusted.

The energy level diagram (Fig. 2-5) demonstrates the DNP mechanism on a single pair of electron and nucleus coupled together. Chapter 1.1 shows that resonance for an electron is at GHz range whereas resonance for proton is at MHz range, therefore under normal circumstances, only single transitions are allowed, represented by blue arrows [12] Either the electron (irradiation at GHz frequencies) or proton (MHz frequencies) may be promoted to higher energy state after interaction with radiation.

Usually, the red transitions are strictly forbidden. However, the hyperfine coupling between the spins is of sufficient magnitude that the 4 energy levels are not pure states, and consequently these transitions become partially allowed [12]. Hyperfine coupling is caused by the interaction between the magnetic moments arising from the spins of both the nucleus and electrons in atoms. In a single electron system, the electron with its magnetic moment moves within the magnetic dipole field of the nucleus. This spin interaction in turn causes splitting of the fine structure of

spectral lines into smaller components called hyperfine structure. The hyperfine structure is approximately 1000 times smaller than the fine structure [41].
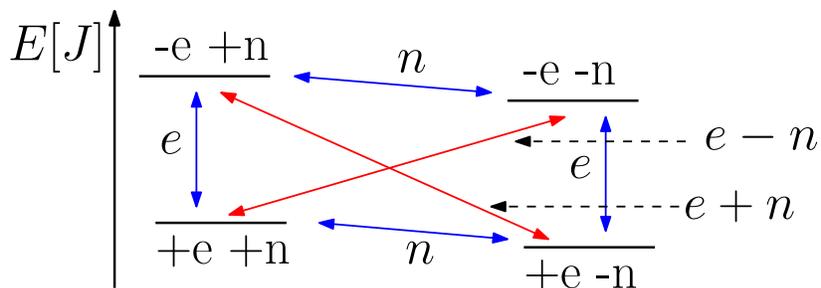

Fig. 2-5   Energy level transitions (Single transition – blue; DNP polarization - red) Energy transitions associated with electrons are higher than nuclear transitions according to equation 2.2 in chapter 2.2. Energy captured by an electron from the radiation in the GHz range is greater than the energy received by proton from the MHz region.

There is pressure to discover and synthesize radicals with as fast relaxation times as possible. These radicals may transfer their polarization via hyperfine coupling to nuclei repeatedly and raise the excited population of nuclei even by tens of per cent, which will then lead to the relaxation of a larger mass of nuclei eventually resulting in a substantially increased signal intensity.

4. Instrumentation

In the following chapter the main focus is going to be dedicated to the description of the theory around High Field EPR (HF-EPR), different methods of scanning of the samples and at the end also to the hardware installed and used in the THz spectroscopy laboratory at CEITEC BUT.

3.1 Field-domain versus Frequency-domain EPR

There are two main streams in performing an EPR experiment. As we already know the Landé factor (g-factor) is a specific fingerprint for every studied element. When I combine the equations 2.2 and 2.5 and express g-factor into equation 3.1

$$g = \frac{h \cdot \nu}{m_s \cdot \mu_B \cdot B_0} \qquad (3.1)$$

Where: h (Planck constant) m_s (spin projection) μ_B (Bohr magneton) are all constants the g-factor becomes the dependent variable on two independent variables: frequency ν and magnetic field B_0. From equation 3.1 arises two methods of EPR scanning, frequency and field domain.

The frequency-domain EPR is the way of experimenting while the external field B_0 is set to the fixed value and frequency is swept through the spectrum to find and match resonance (see Fig. 3-1A). This method may be quite challenging on microwave source which is expected to be able to produce constant mw power and steady change of microwave frequency throughout the whole spectrum.

The second possibility is to lock microwave frequency and change the magnetic field at a steady pace. At a certain point, the strength of the magnetic field reaches the ideal value for observing resonance (see Fig. 3-1B). This method, called field domain, is more common but on the other hand, the experiment duration is prolonged due to the necessity of a much slower sweep with the magnetic field in contrast to the possible speed of frequency speed.


(A)   (B)
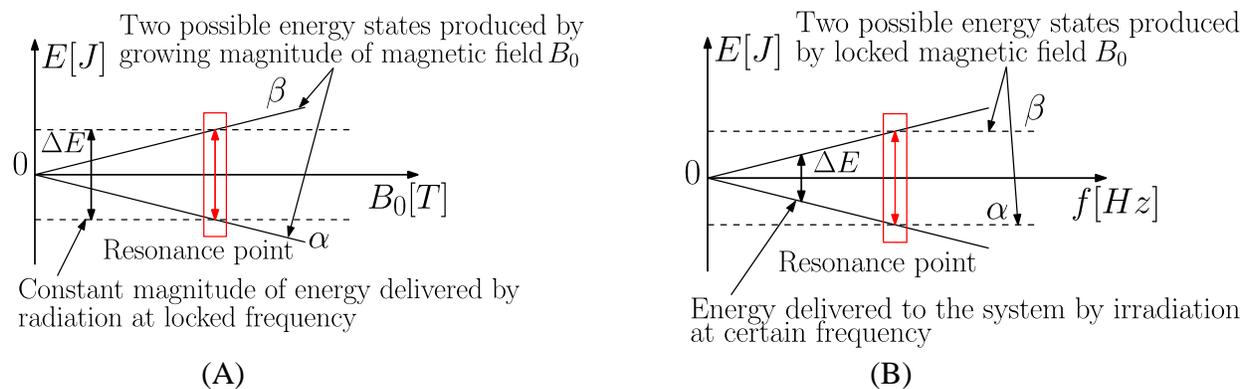
Fig. 3-2   A) Visualization of the frequency domain, steady magnetic field producing two possible states α and β. Increasing microwave frequency delivers larger and larger quanta of energy until the resonance point is reached. B) Field domain approach. The energy delivered by microwave radiation is of the same magnitude, whereas the growing strength of the magnetic field increases the difference between states α and β until it matches desired ΔE.

4.1 Reason for High-Field EPR

The previous section discussed two possible methods of differentiating the energy levels and this part gives the main benefits of utilization of the high field (HF) at low temperatures.

As the sample consists of thousands of molecules it would not be a wrong assumption arising from classical physics on a macro scale that the system favours the energy state with lower energy. However, while dealing with molecules having such small dimensions one needs to consider the point of view of quantum physics, which describes the systems rather by the possibility of molecules occupying a certain energy level. At temperatures close to absolute zero, we would indeed predict that the vast majority of spins would have quantum amplitudes vastly favouring the lower energy (parallel) state. At room temperatures, however, this tendency for spins to prefer the lower energy level is opposed by thermal motions that tend to equalize the two energy levels. The resultant equilibrium distribution is therefore a compromise predicted by the Boltzmann distribution [19].

$$\frac{N_\beta}{N_\alpha} = \exp\left(-\frac{\Delta E}{kT}\right) \qquad\qquad 3.2$$

Where N_β is the number of molecules occupying the antiparallel state; N_α is the number of molecules occupying the parallel state; ΔE is the energy difference between states; T is the thermodynamic temperature in Kelvin and k is the Boltzman constant $k = 1.380\ 658 \cdot 10^{-23}$ [7]

For the ratio $N_\beta / N_\alpha \approx 1$ there is almost no difference in the population of different energy levels which means that no absorption may be detected. This implies that for the ideal absorption it is optimal for this ratio to be as close as possible to 0, which it does at a high magnetic field and the temperatures close to $0\ K$. The following table 3-1 compares the ratios of different frequency bands at room temperature and the temperature very close to $0\ K$. However, the ratio drops slightly due to a stronger magnetic field even at room temperature, the most significant drops come with lowering the temperature as well. For instance ratio at room temperature for Y-band is almost 1:10, but for $2\ K$ it drops down to 1:2000, which promises considerably larger absorption.

Tab. 3-1; Occupancy rate of energy levels α and β at different frequency bands and temperatures

Frequency band	Frequency [GHz]	Magnetic field [T] for $g = 2$	$\frac{N_\beta}{N_\alpha}$ at $293\ K$	$\frac{N_\beta}{N_\alpha}$ at $2\ K$
X-band	9.6	0.343	998/1000	794/10^3
Q-band	35	1.250	994/1000	432/10^3
W-band	95	3.394	984/1000	102/10^3
Y-band	420	15.004	934/1000	42/10^5

The next benefit of the application of the HF-EPR is for the samples consisting of two or even more species with dissimilar g-factors. At lower frequencies, it may be very complicated to distinguish these two different signals in EPR spectra. Nevertheless, the HF-EPR has a higher resolution which may even completely separate these two signals from each other. Fig. 3-1 demonstrates how the resolution increases with a stronger field and higher frequency.
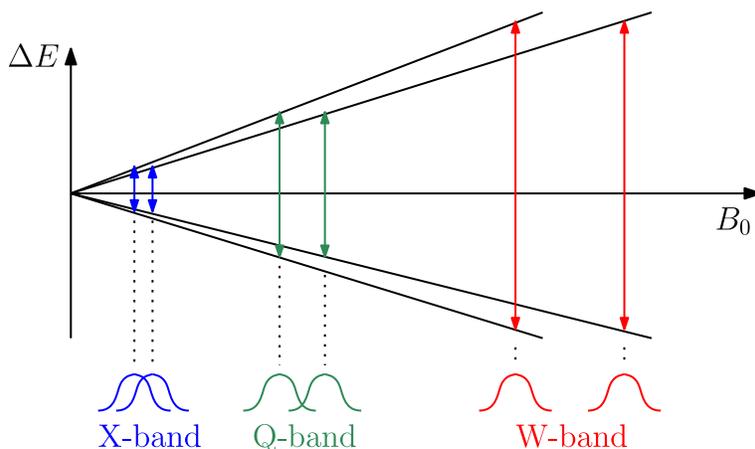

Fig. 3-1   Two species of different g-values are very difficult to distinguish at the X-band frequency. The situation is better for Q-band, but the lines are fully separated only for W-band [2].

The third benefit is the recognition of a hyperfine coupling from two species with different g-factors. It was explained how the HF-EPR enhances resolution and separates the overlapping signals. But there may be signal-splitting not only due to dissimilar g-factors but also due to hyperfine interaction between electron and nuclei. The nuclei of the atoms in a molecule or complex have a magnetic moment, which produces a local magnetic field at the electron. The magnetic moment of the nucleus acts like a bar magnet and produces a magnetic field at the electron, B_I. This magnetic field opposes or adds to the magnetic field from the laboratory magnet, depending on the alignment of the moment of the nucleus [6]. When B_I adds to the magnetic field, less magnetic field is needed from the magnet and therefore the field for resonance is lowered by B_I and vice versa. Fig. 3-2 shows signal split for a spin 1/2 of a hydrogen nucleus.

Very important is that this distance B_I is independent of the strength of the magnetic field. In HF it is possible to distinguish if the split is caused by the different g-factors or by the hyperfine interaction
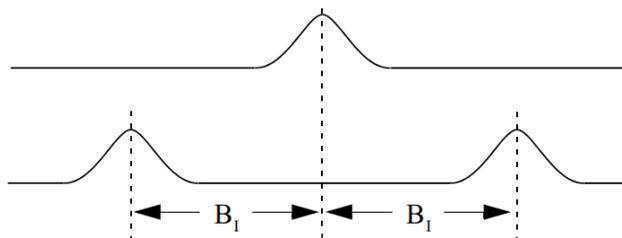

Fig. 3-2   Figure taken from [6] and adjusted. The spectral split by hyperfine interaction

4.2 EPR scanning methods

Continuous-wave EPR spectra are recorded by putting a sample into a microwave irradiation field of constant frequency ν and sweeping the external magnetic field B_0 until the resonance condition is fulfilled [21]. Such measurement may be used for instance in finding the exact value of the resonance point. There may be calculated a theoretical expected resonance point in advance and after that, the cw EPR spectra of a particular sample is recorded by slow sweep with magnetic field in the adjacent surrounding of theoretical B_0 value. From this experiment, the resonance point is either confirmed or slightly corrected and adjusted to actual conditions.

In pulse EPR the spectrum is recorded by exciting a large frequency range simultaneously with a single high-power mw pulse of given frequency ν at a constant magnetic field B_0. However, there are certain technical limitations in the pulsed method. During and immediately after the MW pulse, the sensitive detector must be protected from the high mw power in the resonator, and signal recording is not possible. This so-called dead time of the spectrometer depends on the bandwidth of the resonator and for instance, at X-band, it is in the range of $100\ ns$ [21]. Pulsed EPR techniques such as electron spin echo envelope modulation or pulsed electron-nuclear double resonance can reveal the interactions of the electron spin with its surrounding nuclear spins [22].

In the first described method cw EPR, the magnetic field is scanned slowly through the resonance but on the contrary the rapid scan (rs) EPR is the cw EPR method where the magnetic field or in most cases the frequency is repeatedly scanned through the spectrum at rates that are much faster than in conventional cw EPR. Rs EPR is particularly advantageous when the scan rate through resonance is fast relative to electron spin relaxation rates. In such scans, there may be oscillations on the trailing edge of the spectrum. These oscillations can be removed by mathematical deconvolution to recover the slow-scan absorption spectrum [23] (see Fig. 3-2). On one hand, rs EPR demands more complicated math and data processing in the background but on the other hand, it offers great benefits such as the slow-scan spectra with much higher resolution than cw EPR, absence of dead time unlike the pulsed EPR and access to the shorter relaxation times. All of these advantages are possible because the spin system can handle much higher excitation power with no visible saturation than in a conventional slow sweep experiment [24]. Those are the reasons why it is the point of our great interest.
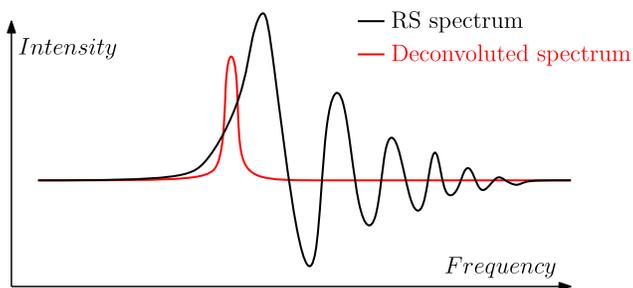

Fig. 3-2   Rapid scan spectrum before and after mathematical deconvolution

The calculation of the spin relaxation times is based on modified Bloch equations. The Bloch equations are a set of macroscopic equations that are used to calculate the nuclear magnetization $\boldsymbol{M} = (M_x, M_y, M_z)$ as a function of time when relaxation times T_1 and T_2 are present [46].

Modified Bloch equations:

$$\frac{dM_x}{dt} = \frac{-M_x}{T_2} - [\Delta\omega + f_m(t)]M_y \tag{3.3}$$

$$\frac{dM_y}{dt} = [\Delta\omega + f_m(t)]M_x - \frac{M_y}{T_2} - \gamma B_1 M_z \tag{3.4}$$

$$\frac{dM_z}{dt} = \frac{M_o}{dt} - \frac{M_z}{T_1} + \gamma B_1 M_y \tag{3.5}$$

Where $\Delta\omega$ is the offset of a spectrum from the centre of the sweep, $\gamma = -1.7608 \cdot 10^7 \, rad/(s \cdot G)$ is the electron gyromagnetic ratio, B_1 is the microwave magnetic field [47]. A deeper analysis of the equation is in [47] by Dr Oleksii Laguta. For the calculation of relaxation times will be used software based on these equations and made also by Dr Oleksii Laguta.

The rapid scan method has one crucial condition which must be met. The frequency of the sweep must be substantially larger than the relaxation time of the sample.

$$\frac{df}{dt} \ll \frac{1}{T_2^2} \qquad\qquad \frac{df}{dt} \approx \frac{1}{T_2^2} \qquad\qquad \frac{df}{dt} \gg \frac{1}{T_2^2}$$

A)   B)   C)
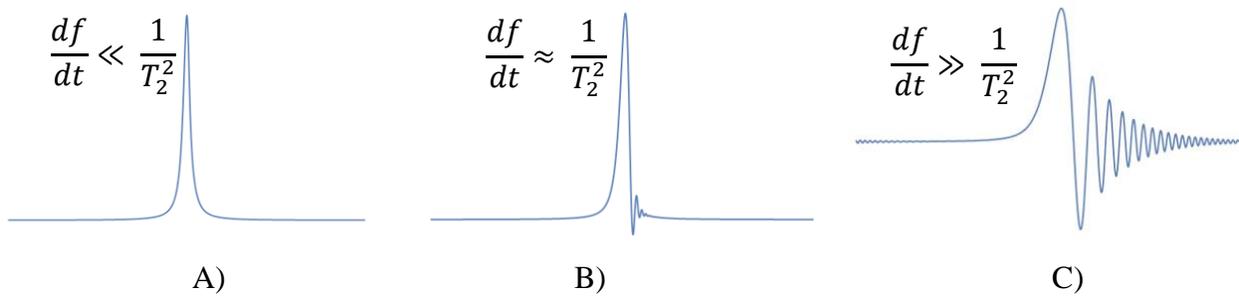
Fig. 3-3   A) Condition for the rapid scan was not met and the recorded spectrum is classical frequency domain sweep. B) The speed of a frequency sweep rises but still is not enough. C) Condition for the rapid scan method is met and the frequency sweep is considerably larger than the relaxation time hence the rapid scan spectrum may be recorded and observed. Pictures taken and adjusted from [47]

4.3 Hardware in CEITEC BUT

The major topic of the following chapter is going to be the essential parts and components of the spectroscope in the magneto-optical laboratory at CEITEC BUT. At first, there is going to be the actual visual representation of the spectroscope (Fig. 3-3), then the model with the essential components and the path of the mw radiation (Fig. 3-4) which should give the reader a closer sense of the component layout and its function.

In the figure (Fig. 3-3) there is a picture of the spectroscope. Note that the EPR spectroscope is an assembly of two parts, magnet frame and movable EPR table with the quasi optics. In the figure, the table is not currently above the probe insert in the magnet so-called loading position, which means that no measurements may be executed at the moment. However, at this stage, most of the maintenance, diagnostics and adjustment of the hardware might be done.
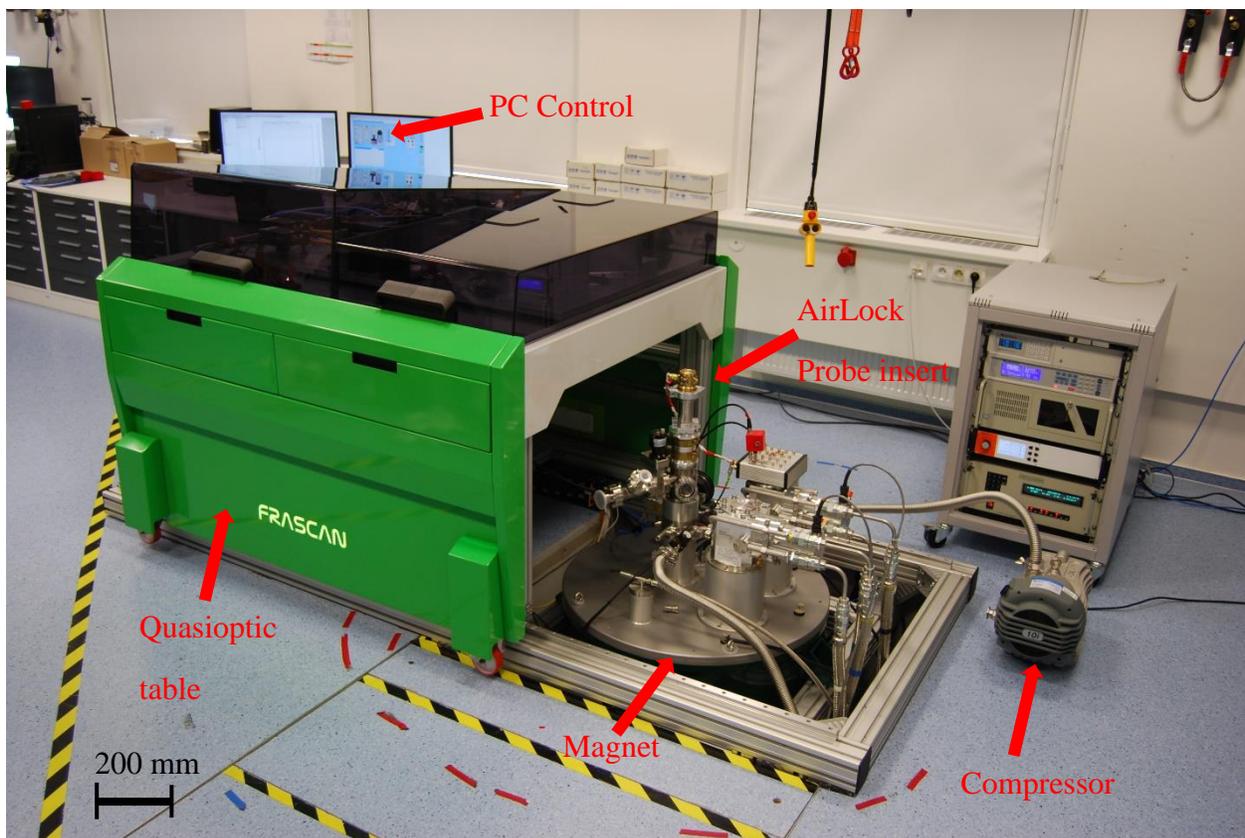
Fig. 3-3   Frequency Rapid Scan Electron Spin Resonance spectroscope (FRASCAN) Actual spectroscope set up as of March 26 2021

The following scheme (Fig. 3-4) represents the model of the actual spectroscope with an indication of the crucial components.
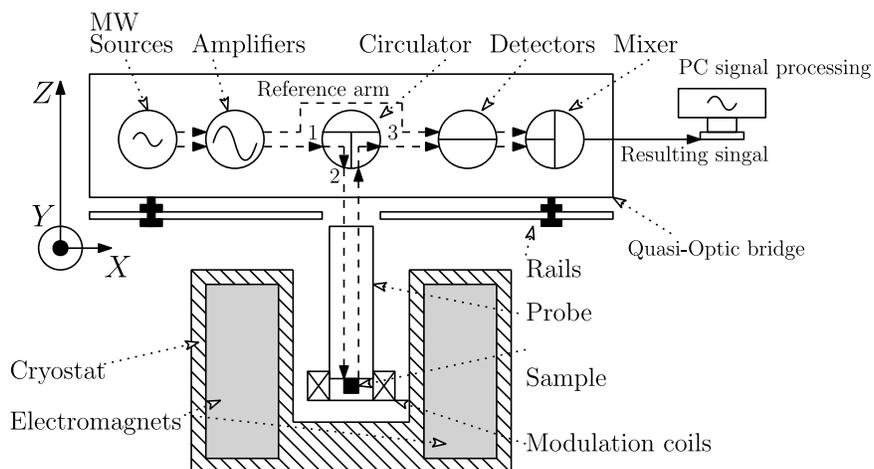
Fig. 3-4   Scheme of the spectroscope hardware with the mw radiation path

The upcoming paragraphs describe all the individual parts. For simplicity, the description will follow the path of the beam from the source to the computer signal processing.

MW Sources: Most millimetre and submillimetre mw sources for EPR spectroscopy can be divided into two groups: vacuum-tube oscillators and solid-state oscillators. Vacuum-tube oscillators such as klystrons, BWOs, gyrotrons, extended interaction oscillators (EIOs) and magnetrons have been and still are used as coherent mm-wave sources. They are, however, increasingly replaced by solid-state oscillators, which are smaller, easier to operate and reach excellent performance with increased reliability [1]. There are used two synthesizers as a source of microwaves capable of the frequency sweep. One as a measurement beam and the second as a reference arm.

Amplifiers: For frequencies above the sources' capability, it is necessary to employ one or more stages of frequency multiplication [1]. This is where the mw amplifiers play an important role. Not only they can boost the mw to the desired frequency, but they also dampen down higher orders of harmonic frequencies.

Circulator: A circulator is a passive, non-reciprocal three or four-port device that only allows a microwave or radio-frequency signal to exit through the port directly after the one it entered [25]. The circulator is crucial in terms of handling the beam propagation. The mw radiation produced and amplified enters port 1 (port numbers are at Fig 3-4) and exits from port 2 right into the sample. When any part of given radiation is reflected from the sample to the circulator's port number 2 it does not come back to port 1, however, it exits from port 3 and travels right to the detector.

Detectors: The end part of the beam is in detectors. The most widely used in EPR applications are bolometers. Bolometers are based on resistive temperature sensors. A bolometer detects electromagnetic radiation by absorption of radiation that increases its temperature. A small ΔT gives rise to a large resistance change ΔR [26].

There is also an alternative and the second very popular stream in detector devices in EPR spectroscopy and it is a Schottky diode-based method. Schottky diode detectors have long been used at mm and submm-wavelengths because of their high sensitivity, their ability to operate at ambient or cryogenic temperature and their fast response time compared with other room-temperature detectors [27]. Schottky diodes are more popular in pulsed EPR due to their fast response time, unlike the bolometers which are rather applied in field-domain experiments for the sake of their slow response time.

Mixer: A mixer is a three-port component, which performs the task of frequency conversion. Two of a mixer's three ports serve as inputs, while the other port serves as an output port. An ideal mixer produces an output that consists of the sum and difference frequencies of its two input signals. In other words: $f_{out} = f_{in1} \pm f_{in2}$ [28].

Probe: A probe is a long tube that has the **sample** attached at one of the ends. The end with the sample is inserted into the cryostat. The important part about the probe is not only the part with the sample but its cavity as well. Microwave cavities are used for amplifying weak signals from the sample. A microwave cavity is simply a metal box with a rectangular or cylindrical shape that resonates with microwaves much as an organ pipe resonates with sound waves. Resonance means that the cavity stores the microwave energy; therefore, at the resonance frequency of the cavity, no microwaves will be reflected, but will remain inside the cavity [6].

Modulation coils: EPR spectroscopists use a technique known as phase-sensitive detection to enhance the sensitivity of the spectrometer. The advantages include less noise from the detection diode and the elimination of baseline instabilities due to the drift in DC electronics. The detection scheme works as follows. The magnetic field strength which the sample sees is modulated (varied) sinusoidally at the modulation frequency. If there is an EPR signal, the field modulation quickly sweeps through part of the signal and the microwaves reflected from the cavity are amplitude modulated at the same frequency. For an EPR signal which is approximately linear over an interval as wide as the modulation amplitude, the EPR signal is transformed into a sine wave with an amplitude proportional to the slope of the signal [6].

The signal channel (more commonly known as a **lock-in amplifier** or phase-sensitive detector) produces a DC signal proportional to the amplitude of the modulated EPR signal. It compares the modulated signal with a reference signal having the same frequency as the field modulation and it is only sensitive to signals which have the same frequency and phase as the field modulation. Any signals which do not fulfil these requirements (i.e., noise and electrical interference) are suppressed [6].

Thanks to a lock-in amplifier's ability to extract very small signals buried in noise, it is possible to expand the reach of experimental setups. The working principle of a lock-in amplifier, called demodulation or phase-sensitive detection, rests on mixing the measured signal with a reference frequency followed by low-pass filtering [29].

Cryostat and electromagnets: The end of the probe with a sample is inserted into the cryostat with large electromagnets. These electromagnets produce a homogenous magnetic field with a precisely defined direction. The strength of the magnetic field may reach up to $16\,T$. To produce such a magnetic field immensely large current flows through the electromagnets. This being the reason they must be cooled down under the $10\,K$ to guarantee superconductivity. To ensure such low temperatures the cryostat takes part in. A cryostat is a machine that maintains the cryogenic temperature of samples or devices placed inside it. Cryostats use several refrigeration methods to achieve low temperatures, such as a helium bath with liquid helium or liquid nitrogen [30].

The last but not least and very important components for this thesis are Bosch Rexroth **servo motors**. These servo motors enable manipulation with the **quasi-optic bridge** (which houses the mw sources, detectors, amplifiers etc.). Spectroscope in THz laboratory at CEITEC BUT is equipped with 5 synchronous servo motors giving the system 5 degrees of freedom which the three of them being the movement along the axis x, y, z and the other two tilts around x, y axes (axes sketched on Fig. 3-4). These servos are controlled via LabView. Bosch Rexroth encourages this type of handling supporting it with regular updates of their library eal4LABVIEW.

5. Gaussian beams

In the fourth chapter, I am going to shed some light on the Gaussian beams. The first part will be more explanatory including the propagation of Gaussian beams and essential theory. The second part will cover more of the application of the theory as well as arising problems with the coupling of such beams. This part is essential because the spectroscope in the Magneto-Optical lab is very unique. As the figures (Fig. 3-3 and Fig. 3-4) show, the optical bridge is placed on top of the rails which enable its movement. However, that is the reason why it is crucial to recouple the optical bridge with the probe below every single time the probe is inserted. There are high demands on the quality of coupling because the coupling quality itself directly affects the signal intensity hence the resultant quality of measurement.

5.1 Electromagnetic radiation

Electromagnetic radiation (ER) is an inseparable part of the universe and the nature around us. The basic concept of ER is that it is the flow of the energy at the universal speed of light through free space or through a material medium in the form of the electric and magnetic fields that make up electromagnetic waves [13].

The characteristic quantity of every ER is its wavelength or frequency which are dependent on each other as shown in equation 4.1.

$$\lambda = \frac{c}{\nu} \tag{4.1}$$

Where λ is the wavelength, ν is the frequency and $c = 299\ 792\ 458\ m/s$ [7] is the speed of light.

There is a broad spectrum of ER beginning with radio wave with a wavelength of kilometres even tens of kilometres. Then as the wavelength shortens and the frequency and energy of radiation grow (equation 2.2), there are microwaves which prefix indicates its wavelength is in micrometres. Then there is a region of visible light in nanometres after which we get to the highly energized and radioactive radiation such as x-rays and gamma rays with the wavelength of hundreds and even as low as tens of picometers.

Every ER incorporates an electric and magnetic component; therefore, the ER is a fusion of these two waves, which undulates in perpendicular planes to each other. The direction of the ER propagation and the magnitude of the flow of the energy is described by the Poynting vector $\vec{S}$ (eq. 4.2).

$$\vec{S} = \frac{1}{\mu_0}\ \vec{E} \times \vec{B} \tag{4.2}$$

The Poynting vector $\vec{S}$ is defined as to be equal to the cross product of $1/\mu_0$ times the electric magnetic field $\vec{E}$ and magnetic field $\vec{B}$, where μ_0 is the permeability of the medium through which the radiation passes [14].

The direction of beam propagation at velocity c (direction of Poynting vector $\vec{S}$) may be found by the right-hand rule at any combination of vectors $\vec{E}$ and $\vec{B}$. Let the fingers of the right hand follow the vector $\vec{E}$, twist them into the direction of $\vec{B}$ then the thumb points in the same direction as the $\vec{S}$. It is necessary to keep the right order of vectors, the first one electric then magnetic.

5.2 Particle and wave approach to radiation

With basic ER theory covered in chapter 4.1 we know, what the radiation consists of and in which direction it propagates. However, there are several approaches simplifying the concept of propagation of radiation.

A first straightforward concept is a geometrical approach which assumes the radiation is a flow of particles (at some point even just a centre of mass without any dimensions) obeying the classical mechanical approach of physics, which is very useful in optics, particularly for example in tracking ray's trajectory via optical frameworks. Geometrical optics is a branch of optics where light is described by rays. Light rays are conceived as geometrical lines originating from sources, extending through media, and being revealed by detectors; their directions account for paths along which light flows [15]. In certain applications this approach with its principles is handy. However, it completely ignores the wave nature of the radiation from wave-particle duality.

All physical entities have a dual character; they are waves and particles at the same time. Everything we used to regard as being exclusively a wave has, at the same time, a corpuscular character, while everything we thought of as strictly a particle behaves also as a wave [16]. The behaviour of the entity will depend on an experiment or rather a feature we would like to observe. In above mentioned geometrical optics the light (or any other ER) behaves strongly as a flow of particles, nevertheless Gaussian beams or even their coupling demands taking into consideration the wave character of ER as well as wave phenomena bounded to it such as interference, diffraction etc.

5.3 Characteristics of Gaussian beam

Now that I have explained all the essential theory behind the ER propagation it is time to shed some light on the Gaussian beam. The best example is light emitted by LASER, which is a source of monochromatic ER in the visible spectrum, but the theory may be applied also on microwaves or any other radiation outside of the visible spectrum. I have chosen a LASER for its easy imagination.

After producing light with a given power, the ray on its own tends to diverge and lose its intensity (irradiance profile starts to broaden Fig. 4-2) due to diffraction and the overall wave nature of ER.
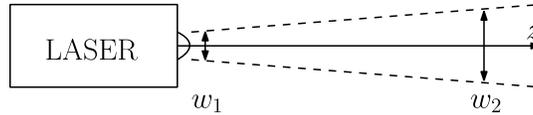
Fig. 4-2   Broadening waist $w(z)$ with increasing distance from the source of the radiation due to diffraction

The intensity of the beam is given by equation 4.3 which is dependent on the power of the ER source P, radial distance r from the centre point in the perpendicular plane to the direction of propagation and the beam waist $w(z)$ which is dependent on the z which is the distance from the source in direction of the propagation.

$$I(r) = \frac{2P}{\pi w(z)^2} \exp\left(\frac{-2r^2}{w(z)^2}\right) \qquad 4.3$$

The waist of a Gaussian beam is defined as the location where the irradiance is $1/e^2$ (13.5%) of its maximum value [17].

However, there are possibilities for how to adjust the beam and gain the intensity. The ray passing through the lens or the system of lenses may be focused, which means shrinking the waist to minimal possible value of w_0 into the focal point f (see Fig. 4-3) thus receiving higher intensities for possible detection.
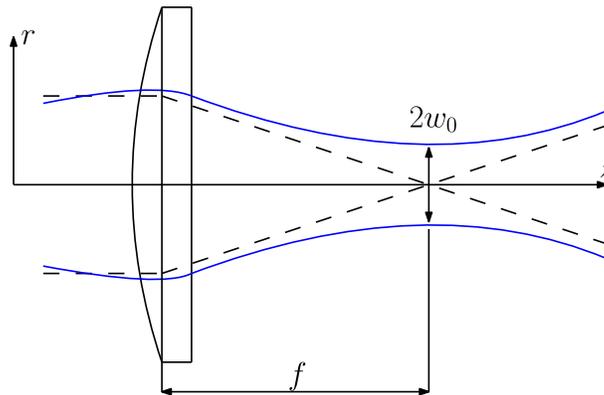
Fig. 4-3   Beam focused by the converging lens into the focal point f where the beam waist w_0 reaches its lowest value

Theoretically, it would be ideal to focus all the radiation into one point, that way we would get the intensity approaching infinity. Nevertheless, this is not possible due to the undulation, so we are limited to a certain minimal beam waist. As shown in Fig. 4-3 after passing the lens the beam is converging until it reaches its minimal diameter d (while talking about the beams it is common to use term beam waist w which is half of the diameter $d = 2w$) and after that, it diverges again.

Fig. 4-4 demonstrates the intensity distribution in the Gaussian beam. In many laser optics applications, the laser beam is assumed to be Gaussian with an irradiance profile that follows an ideal Gaussian distribution [17]. Although Fig. 4-4 displays only one possible mode of the Gaussian beam, there are more of them that differ from each other by the place of their maximum intensity. Higher orders of Gaussian beams do not have to have only one intensity maximum. The

maximum might also alternate with the minimum; these higher-order Gaussian beams are referred to as different modes.
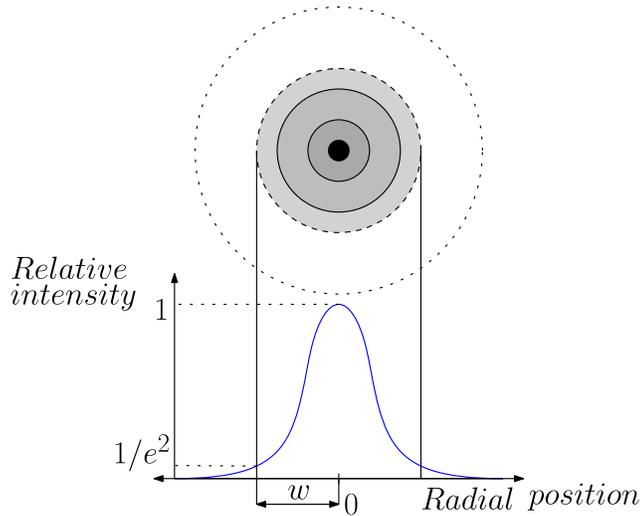
Fig 4-4   Intensity distribution of the Gaussian beam in the mode 0;0. The image was taken and adjusted from [17].

5.4 Gaussian beams coupling

One of the well-known phenomena in wave conception of radiation is interference. If the two or more waves meet each other and they are ideally coherent (waves have the same frequency, same phase difference and same waveform [42]), they interact with each other. There are two ideal types of interference: constructive and destructive. Destructive interference is when two coherent waves meet, and they are in antiphase and cancel each other. On the other hand, there is constructive interference when the resulting wave is a sum of these two waves, which met in phase [43]. This is the principle I would like to incorporate in the coupling of the two beams.

The most crucial issue in designing and setting up a Gaussian beam transfer line is the sensitivity of the system to misalignment. Since in our case, the microwave setup does not consist of one single piece (see chapter 3. Instrumentation), it must be realigned frequently. It is therefore of importance to know which kind of results in the most serious insertion loss and how critical it is [18].

1. Lateral misalignment happens when the central axes of both beams do not lay on each other. In an ideal situation, they should merge and make up only one straight line. Although, there is always at least slight misalignment. In Fig. 4-5A the situation is simplified into the one axis with Δx, however, Fig 4-5B shows the full-sized problem when the misalignment Δr is a two-dimensional problem in the plane perpendicular to the direction of propagation.

A)

B)
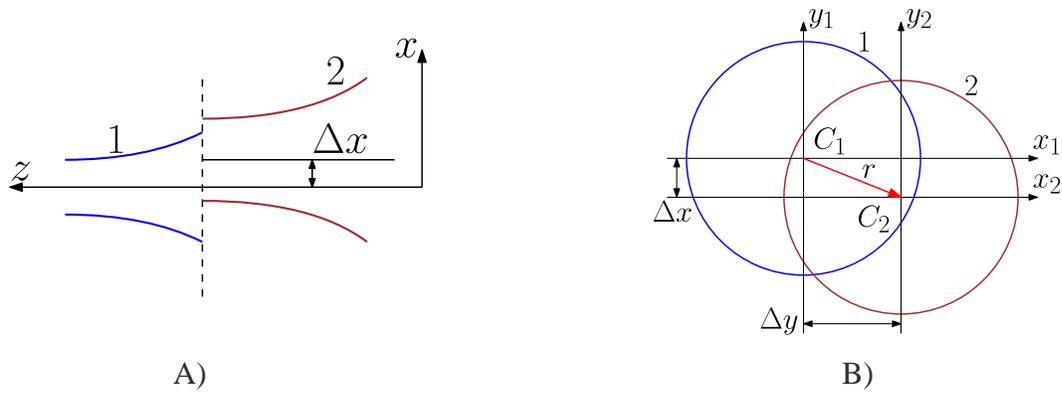
Fig. 4-5   A) Lateral misalignment of beams 1 & 2 by Δx. B) Lateral misalignment in xy plane perpendicular to the direction of propagation with the deviation Δr

2. Longitudinal misalignment describes a situation when despite the central axis are perfectly merged so there is not any lateral misalignment, the beams are not coupled ideally as their minimal waist $w_0(z)$ are at a different z coordinate Δz as it is shown in Fig. 4-6.
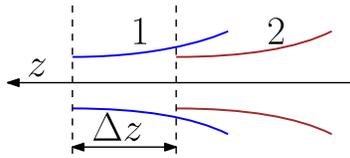
Fig. 4-6   Illustrative demonstration of longitudinally misaligned beams with deviation Δz, the narrowest parts of the beams are at a different z coordinate

3. The third angular misalignment is the matter of the mutual tilt of the beams $\Delta\theta$. Regardless of the flawless correction of the previous 2 misalignments, there is still an urge to ensure both beams are as parallel as possible, and their mutual tilt is approaching zero degrees. The situation is demonstrated in Fig. 4-7.
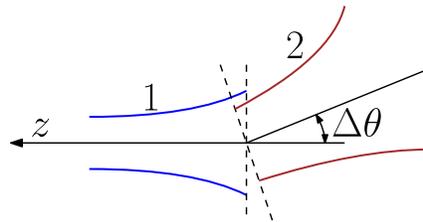
Fig. 4-7   Mutual tilt of two beams with angular deviation $\Delta\theta$

Now that the subject of correct alignment has been introduced, visualized, and classified into three main groups, it is time to add the mathematical description. First thing first there is necessary coefficient K, the coefficient of coupling, which represents the coupling precision, and its value may be within the interval of $< 0; 1 >$, where $K = 0$ indicates total misalignment and loss of power. On the other hand, $K = 1$ represents excellent coupling and ideal constructive interference of the two beams. For each of the three above mentioned misalignments, there is an equation according to [18], which describes dependency among K – coupling coefficient, w_0 – minimal beam waist, λ – wavelength and $\Delta r / \Delta z / \Delta \theta$ - corresponding deviation.

1. Longitudinal coupling coefficient

$$K_{Long} = \frac{4}{4 + \left(\frac{\lambda \cdot \Delta z}{\pi \cdot w_0{}^2} \right)}$$

(4.1)

2. Lateral coupling coefficient

$$K_{Lat} = \exp \left(- \frac{\Delta r^2}{w_0{}^2} \right)$$

(4.2)

3. Angular coupling coefficient

$$K_{Ang} = \exp \left(- \left(\pi \cdot \Delta \theta \cdot \frac{w_0}{\lambda} \right)^2 \right)$$

(4.3)

All the equations above are derived in [18], I have taken only the final form as their application is important for me. Since the spectrometer at CEITEC VUT is used in a variety of frequency bands (from X-band $\approx 10 \; GHz$ up to the Y-band $\approx 420 \; GHz$) it would be helpful to investigate and plot for better visual representation how are different coupling coefficients dependent on the frequency. For this particular reason, I have run simulations in Matlab and plotted the resulting dependency in Fig. 4-8.

Fig. 4-8 is simulated with the beam waist of $w_0 = 9 \; mm$ (actual beam waist value used at CEITEC VUT). However, the following displacements $\Delta r = 5 \; mm$; $\Delta z = 180 \; mm$; $\Delta \theta = 0.03 \; rad$ used in the simulation are intentionally large to illustrate the actual dependency throughout the spectrum.
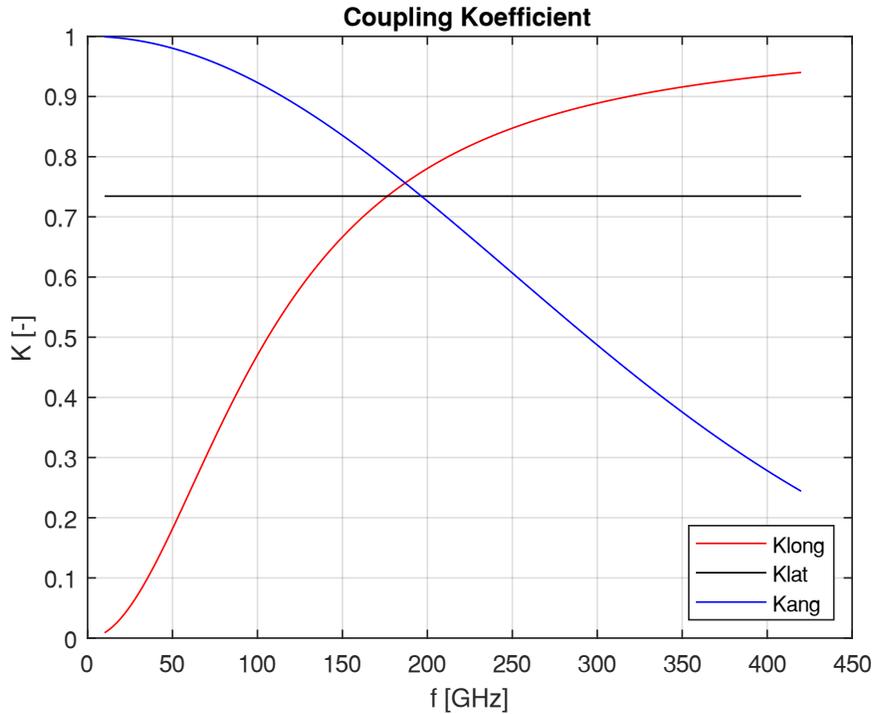
Fig. 4-8   Matlab simulation of different displacements and their dependency on frequency.

From Fig. 4-8 arise very important conclusions. The longitudinal misalignment plays a significant role at lower frequencies. On the other hand, at higher frequencies, the angular misalignment is very problematic. The lateral misalignment is not directly dependent on the frequency based on equation 4.2 and the data from a simulation.

```matlab
clc, clear all

% Beam parameters

w0 = 9e-3;              %beam waist [m]
deltaZ = 180e-3;       %longitudinal displacement [m]
deltaR = 5e-3;         %lateral displacement [m]
deltaFi = 0.03;        %angular displacement [rad]
freq = 10:0.001:420;   %frequency [GHz]  10-420 GHz
c = 3e8;               %speed of light [m/s]
for i = 1:length(freq)
    lambda(i) = c / (freq(i) * 1e9); %wavelength [m]
end

% Dependency of Klong on frequency

for j = 1:length(lambda)
    Klong(j) = 4 / (4 + ((lambda(j) * deltaZ) / (pi * w0^2))^2);
end
plot(freq, Klong,'r');
hold on
clear j;

% Dependency of Klat on frequency

for j = 1:length(lambda)
    Klat(j) = exp (- (deltaR^2 / w0^2));
end
plot(freq, Klat, 'k');
hold on
grid on
clear j;

% Dependency of Kang on frequency

for j = 1:length(lambda)
    Kang(j) = exp (- ((pi * deltaFi * w0) / lambda(j))^2);
end
h = plot(freq, Kang, 'b');
grid on
xlabel('f [GHz]')
ylabel('K [-]')
title('Coupling Koefficient')
legend('Klong','Klat','Kang', 'Location', 'southeast')
clear j;
```

Fig. 4-9   Example of simple Matlab code for simulation of equations 4.1, 4.2, 4.3 with variable inputs of beam waist and displacements for better inspection.

6. Aims of the thesis

1. Description of Rapid scan EPR spectroscopy on DNP relevant radicals

2. Calculations of the relaxation times via rapid scan on radicals

3. Study of the effect of beam coupling on the rapid scan signal

The theory relevant to the goals of the thesis was covered in the theoretical part. The following chapters will address the practical side of the goals. After addressing and implementing solutions there will be a part for comparison and evaluation of the results and final discussion with possible improvements for the future.

7. Testing holder

The first practical task will further describe the purpose, design, and implementation of the testing holder for the probe outside of the cryostat.

The main motivation for this enhancement is that the current spectroscope setup is equipped only with the main insert (see Fig. 3-3). It means that every single measurement or even simple test and maintenance must undergo full loading and unloading procedure, which is time-consuming, especially when needed to apply repeatedly.

The designed testing holder will address all these problems. Such a piece of equipment will serve for experiments that do not require a magnetic field. It may be also used for any maintenance or calibration, but most importantly for this thesis, it could be used for development and further enhancements of the automated coupling mechanism.

Testing holder will be also useful for the time when the magnet is broken down. Situations, when the magnet is not functioning, occurs from time to time. At that moment testing holder may be used for experiments that do not require a magnetic field and the point of measurement is for example recording of the reflected power.

The whole holder consists of several parts numbered in Fig. 6-1. Detailed drawings of each part and drawing of the full assembly are in the attached files.

1 – Fundamental vertical plate

2 – Bottom horizontal plate

3 – Top horizontal plate

4 – Thread

5 – Nut

6 – Bottom sliding bearing

7 – Alutec connection 304343
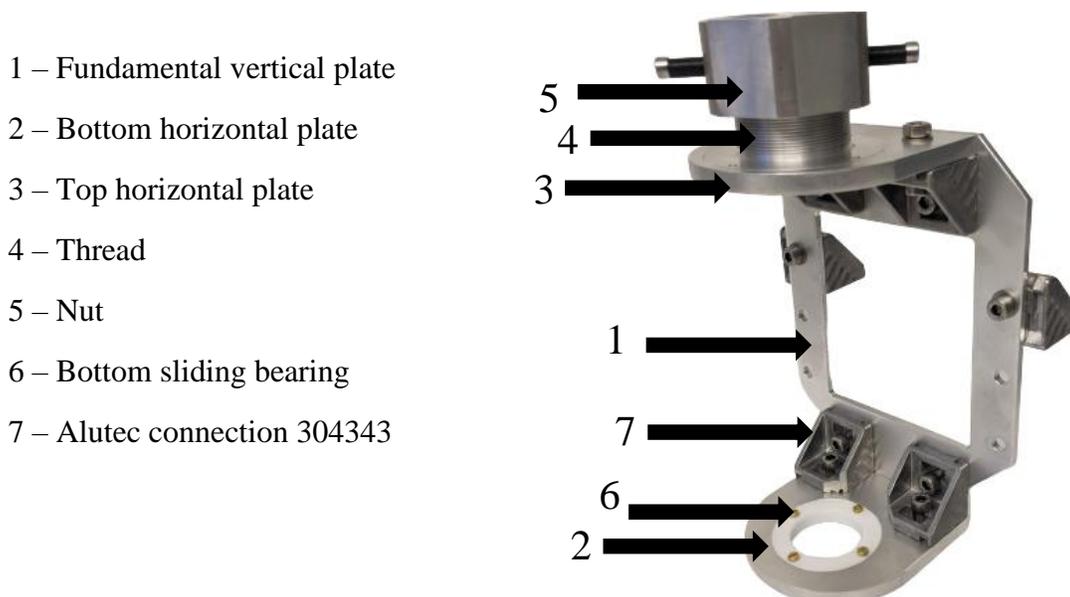
Fig. 6-1   Manufactured and assembled testing holder

The base of the holder is the vertical plate which serves as an attachment to the aluminium beam and the framework itself. It has several holes drilled and prepared for the connection of the two vertical plates with default connection components from the Alutec catalogue. There are also smaller holes for securing pins which ensure geometrical parallelism of both horizontal plates. Each of these plates has a Teflon sliding bearing which ensures smooth and tight insertion of the probe without any scratches and deformations. The top plate, beside the plain bearing, has a tall and hollow thread with its nut. This thread and nut couple have a function of final fine adjustment

of the height of the probe. The thread has a very small lead to minimalize potential unwanted slip due to possible vibrations from the environment.

The whole assembly was mounted to the aluminium beam to a desired spot next to the magnet (Fig. 6-2).
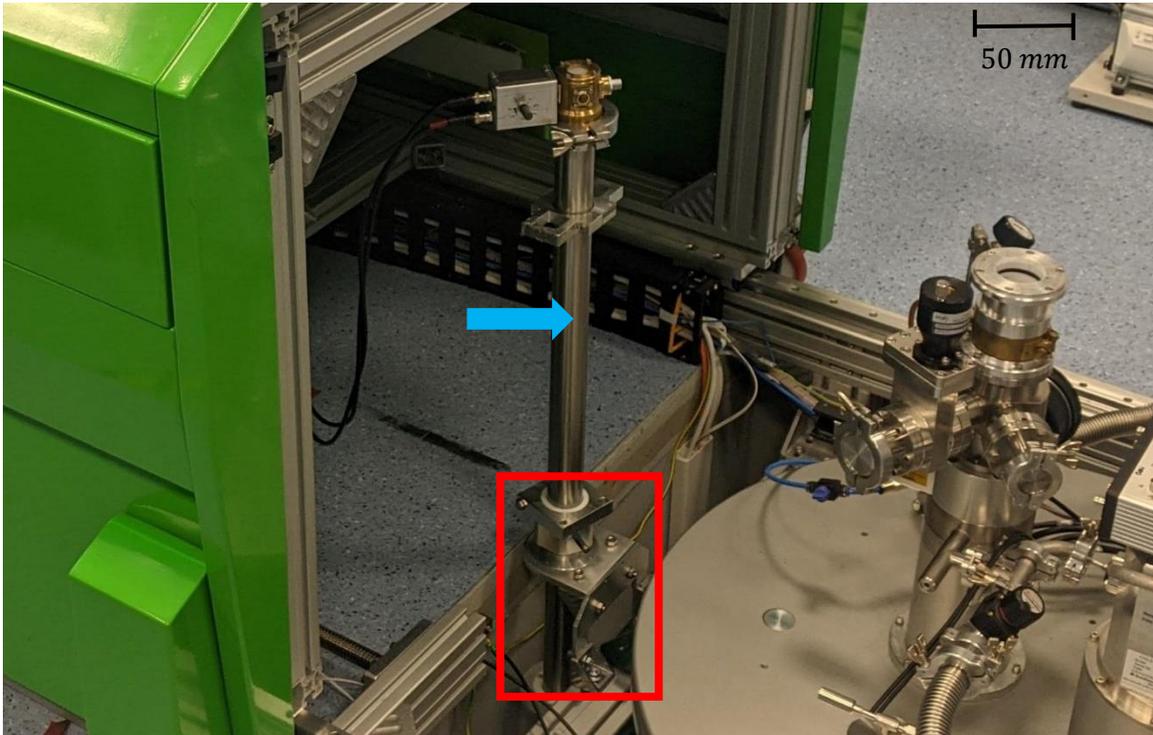
Fig. 6-2   Attached testing holder to the framework (red rectangle) with inserted probe (blue arrow)

8. Automatic coupling system

The development of this algorithm demands splitting the task into several sub-steps. This chapter chronologically describes the individual tasks. Beginning with software communication with hardware for driving servos and processing signal intensity. Then the conceptual solution will be proposed, which will be realized in relevant software, followed by the algorithm implementation into the operation, final fine modifications, and real measurements.

8.1 Communication LabVIEW – Bosch Rexroth servos

Initially, there was a discussion about which software to use. The final decision crystalized as LabVIEW because there is huge support for the interface LabVIEW – Rexroth. Bosch Rexroth develops and updates a library (their addon) named eal4LabVIEW.

The EAL (Easy Automation Library) is a programming interface for high-level programming languages (C/C++/C#/Java/LabVIEW/...). It can be used to write applications to configure and run Bosch Rexroth Drives [44].

Addon eal4LabVIEW includes sub-libraries for connection, parametrization, motion control, … (Fig. 7-1) which then contain direct built-in functions for program construction.

Fig. 7-1   eal4LabVIEW addon

8.2 Communication LabVIEW – Lock-in amplifier

A very similar style of communication works for reading and handling the data from the Lock-in amplifier via LabOne library by Zurich Instruments (Fig. 7-2).
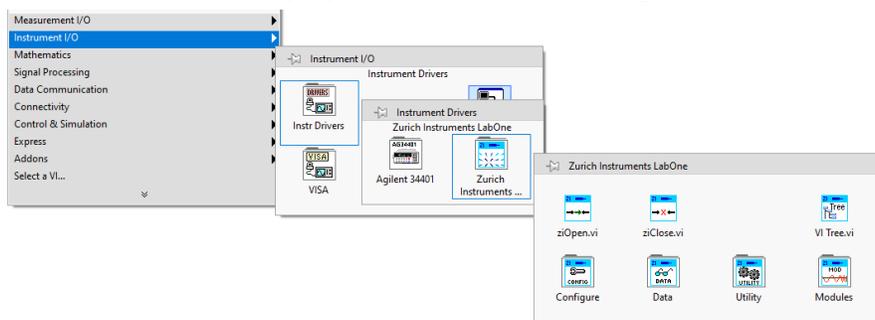
Fig. 7-2   Library for manipulation with data from Lock-in amplifier by Zurich Instruments

Another used interface is LabOne also by Zurich instruments. It is a web interface used for controlling and setting up a Lock-in amplifier's properties. It also enables to plot of the current measured values in real-time as shown in Fig. 7-3.
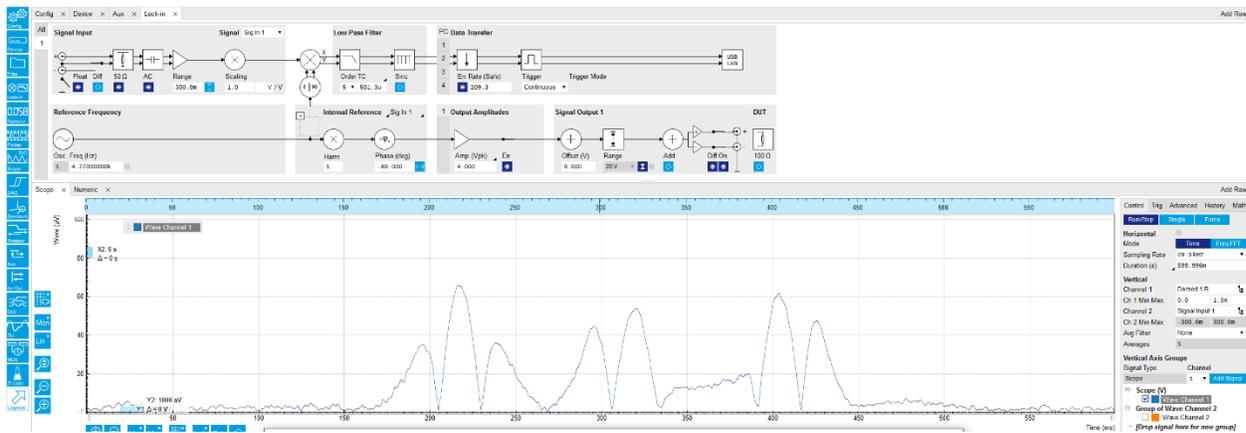
Fig. 7-3   Illustrative figure of LabOne user interface control panel and plot area of signal in real-time

8.3 Coupling algorithm breakdown

The movable table above the magnet is equipped with 5 servo motors. One for the x movement, one for y movement and three for z movement and tilts. The general task is to find the maximum of the intensity function of 5 variables $I = f(x, y, z_1, z_2, z_3)$. Analytically it could be done by partial derivations put equal to zero and after solving resultant system of equations inspecting each point, however, there are a couple of limitations to the analytical approach.

The first limitation of the analytical approach is the human imagination. The function of 5 independent variables has the $n + 1$ dimensional graph (in this particular problem 6D), which is quite frankly impossible to imagine or to plot.

The second and the main problem is that the function is always unknown, so it is impossible to analytically derive an unknown function besides the fact that it would not be a trivial task.

A solution is a numerical approach. In this case, the initial point is that the maximum must be within a given interval (physically circulator above the probe). There are certain intervals for all axes. Fig. 7-4 shows the interval for x, however, the same principle is used for each of them.
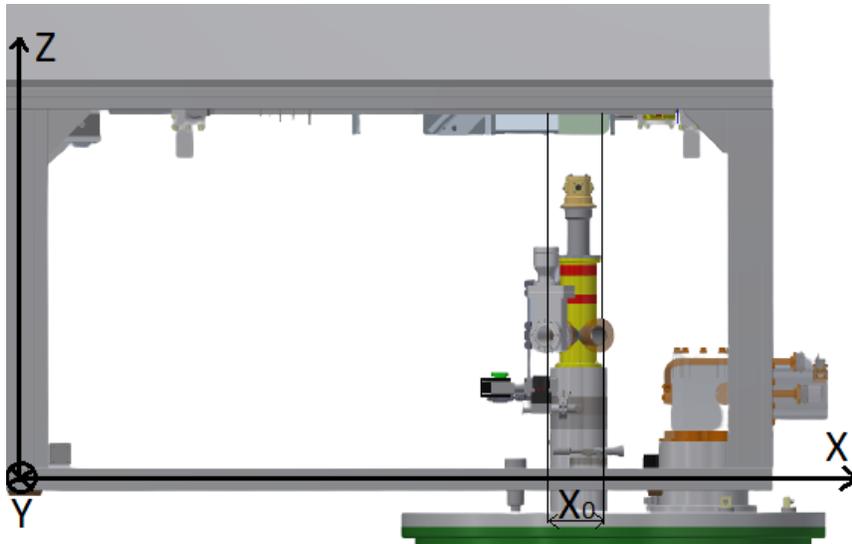
Fig. 7-4   Interval x_0 which contains intensity maximum for x axis

The initial step for the program is to move inside the intervals for obtaining at least some signal. Once all servo motors are set to their let us call it a default position the procedure may begin. Another step is sampling the interval in x and y direction. The action starts with x axis when the table is positioned on the edge of the interval where the signal is of poor quality. The table samples area by $0.5\ mm$ saving the signal intensity into a matrix where to each point a measured intensity is assigned (the quality of the signal is determined by the integral of the plotted area in Fig. 7-3. The plot is made up of a vector sum of the two signals, which means that it is always a positive number. The better the signal the higher is the value of the integral, which makes it very suitable for comparison and evaluation process). In the process, the program assigns the signal intensity to each position and compares its mutual relationship. If the signal improves the sampling continues to another position at $x + 0{,}5\ mm$, if the signal decreases in quality twice in a row (twice in a row to filter out any local maxima and other randomities), it is decided that the maximum for the given interval was found and the table moves back to the position with the best signal. The identical sampling takes place for y direction. This way the x, y axes are roughly coupled for the first time.

The tricky part starts with the movements in the z direction. It is not possible to apply the same mechanism because with every z movement comes inherently tilt of the table which instantly decouples xy plane due to the new beam angle. Because of this issue, it is not possible to instantly compare the obtained values. Very important is that even after a slight z movement the whole x, y coupling procedure must take place again (however this time with a much more fine sampling rate of $0.1\ mm$. Also, now the system does not intentionally decouple that would be counterproductive. This time the table investigates both directions from the current position). Eventually, when x, y are coupled again the signal intensities for z before and after may be compared and evaluated. The following Fig. 7-5 visualizes this crucial problem because of its high importance and the necessity to understand the reasoning behind this procedure.
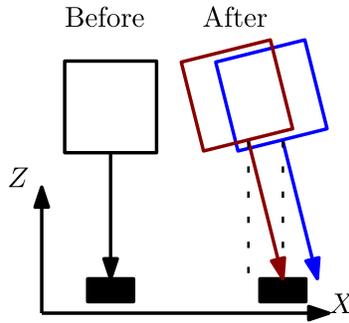
Fig. 7-5   Problem in z direction. Every z movement causes a tilt of the table (From the black *before* to the blue *after*) which needs to be corrected (brown *after*)

This method of coupling is applied to every servo motor with motion in z direction. Nevertheless, the steps are very small ($0.1\ mm$ for both z movement and x, y recoupling). In the case of z the increments are small according to the simulation in Fig. 4-8 which suggest that for the angular misalignments the signal intensity is very sensitive especially at higher frequencies which are predominantly used. The x, y steps are inherently small because decoupling was not that significant due to the small z increment as well as it is beneficial to sample the surrounding area delicately to detect any potential signal enhancements. With this procedure completed, the coupling is considered to be done.

8.4 The code architecture

The code is built programmed in LabVIEW, it is a system-design platform and development environment for a visual programming language from National Instruments. The programming is based on data availability. If there is enough data available to a subVI or function, that subVI or function will execute [45].

Because the code consists of hundreds of blocks, functions, and loops it is impossible to insert a whole code into the thesis or even try to explain it in full detail. Only the most important and/or the most frequent and crucial solutions for some of the problems will be selected and discussed. The full code may be shared after a personal request.

The first part that plays an important role is the piece of code that serves for reading the signal from the Lock-in amplifier and integrating the signal. Fig. 7-6 shows the exact process. There will be selected a couple of blocks (parts) and explained their function so the reader may catch a drift and follow the reasoning behind it.
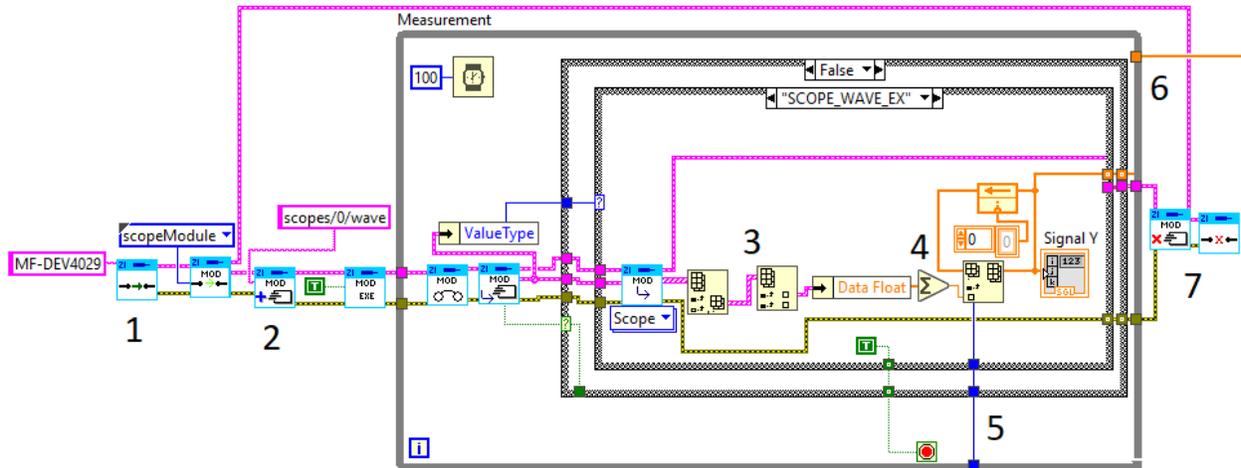
Fig. 7-6   The part of the code for measuring a signal intensity

The number 1 (n. 1) is the connection to the hardware under the given name which is followed by n. 2 which subscribes to the data which are in the buffer. N. 3 is the complex of blocks which at first pulls all the data and filters out only the signal vector. N. 4 integrates it and saves into the matrix at the *n-th* position which is n. 5 that comes from the outer while loop as a number of the iteration. N. 6 is a final integrated number which contains the information about the signal strength. The operation ends with the n. 7 unsubscription and disconnecting from the device. This part of the code is the most used throughout the whole algorithm because every decision which is made inside is based on the knowledge and comparison of the measured signal strength.

On one hand, the knowledge of the signal strength is crucial, however, it must be assigned to the exact position and that is the purpose of the code in Fig. 7-7.
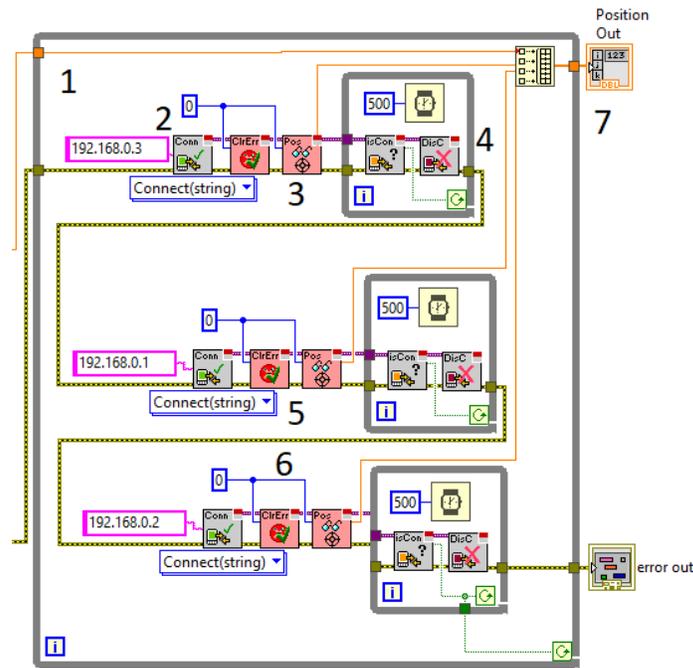
Fig. 7-7   Loop for the assignment of a signal to positions of servo motors

Fig. 7-7 is a very frequently used part of the code. N. 1 is the obtained signal intensity from the previous piece of code (Fig. 7-6). N. 2 is a connection to the desired servo motor at a specific IP address. N. 3 is reading the position from the encoder and sending it to the matrix. N. 4 is the loop for reliable disconnection. Disconnecting loop may seem redundantly extensive, however, if disconnecting process does not run successfully, it generates errors which endanger following attempts for connection. N. 5 and n. 6 are duplicates of the piece above which read the positions from the other two servo motors. N. 7 is the final matrix with the signal assigned to appropriate positions.

The last shown piece of code from those of high importance is the one that builds on the previous two. Fig. 7-8 is the piece of code for moving the servo motor by $0.1\ mm$ in z direction and using subVIs to recouple in x and y direction as well as subVI for measurement and assigning the new data at a new position.
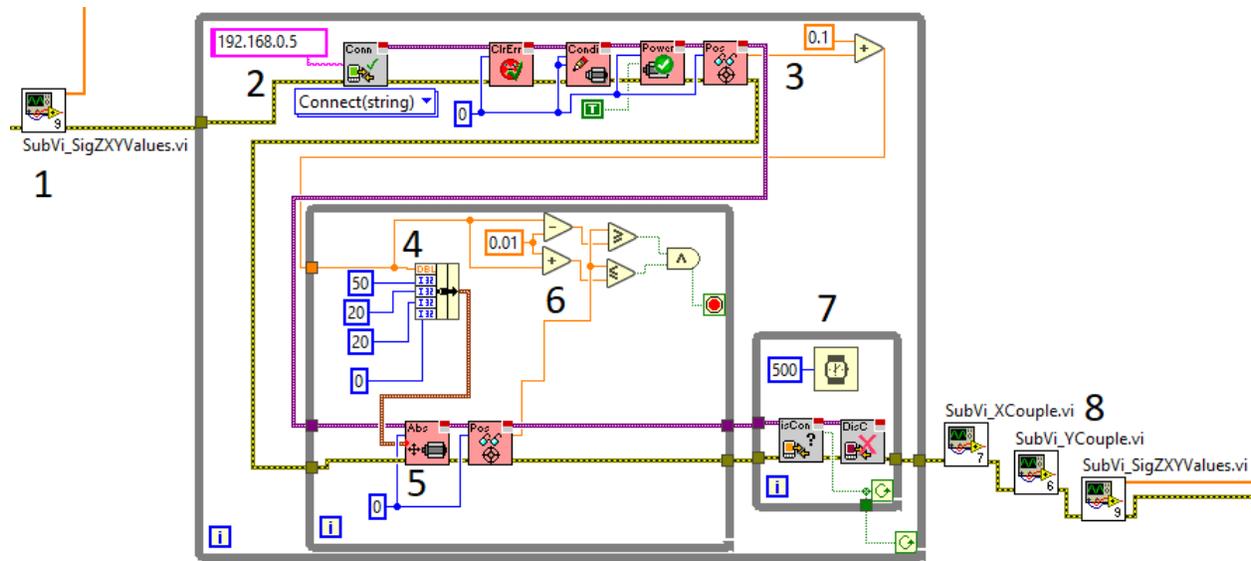
Fig. 7-8   The piece of code responsible for setting up and inspecting the table at the new position

The n. 1 is the piece of code from Fig. 7-7 packed into the subVI from which the signal intensity and position are saved before any movement for further comparison. N. 2 is a connection to the desired servo motor with other necessary procedures such as setting the condition and turning on the power supply. N. 3 is reading the current position and adding a small increment to it which makes up the new position to which the table will be moved. N. 4 is the building of the cluster with all essential conditions for the motor before any movement. It consists of 5 numbers listed from up to down it is a new position, velocity, acceleration, deceleration and jerk. This cluster is passed to the function driving the servo. The loop is completed only when the servo occurs within a given interval built under the n. 6. The new interval is the new position $z \pm 0.01\ mm$. After reaching such a position the end condition for the loop is met and the part under n. 7 is run, which is already explained disconnecting process. The n. 8 are three subVIs, as their names are self-explanatory, one for the x recoupling, the second for the y recoupling and the third for the loading and saving the signal at the new place which is sent for comparison with the position before.

The three very important pieces of the code were presented. These are frequently used throughout the whole code. They are sometimes slightly modified but the structure is very similar. The final code is built from many subVIs and while viewed as complex it does not make much sense at a glance because all the action is divided into smaller sub-blocks. That is the reason why there are presented several subVIs and not the whole code at once. But what may be attractive for the user is the user interface (UI) which is designed to show what is currently going on in the process.

8.5 User interface

The UI is the interface designed for the user to communicate with the program. Designed UI gives the user an overview of the current situation and action control for emergency situations (Fig. 7-9).
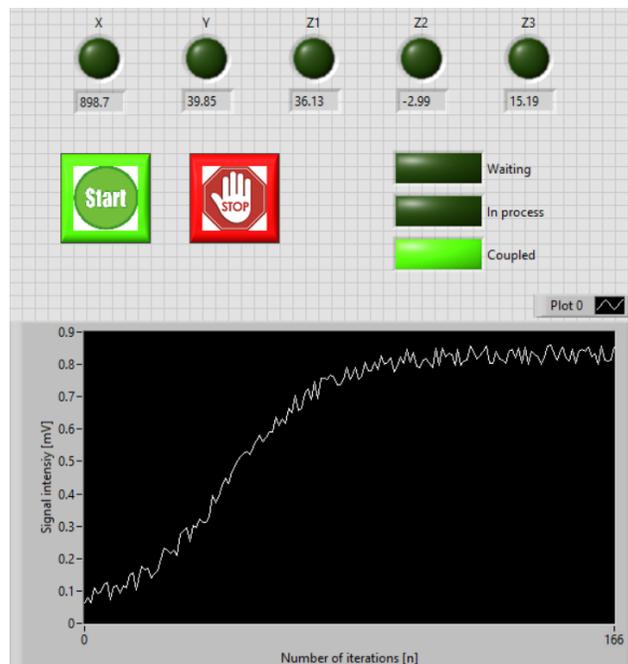
Fig. 7-9   Designed UI for the coupling algorithm.

The UI is designed in a simple manner. It gives a basic overview of the process with a pair of buttons for action. On the top, there are five indicators of servo motor activity (light green means the servo is in the movement). Underneath them, there are numerical indicators of the current position. The only action for the user is two buttons, the starting button and a stop for an instant abortion of the process in case of an unexpected emergency. Next to the buttons, there are three status indicators, so the user is instantly aware of the current situation. The bottom part is reserved for the chart where the evolution of the signal quality is plotted in real-time.

9. Measurements, results and calculations

The last chapter will present achieved results. The first part will be dedicated to the enhancement in the signal intensity in measurements of 4-hydroxy-2,2,6,6-tetramethylpiperidin-1-oxyl (liquid TEMPOL) and rapid scan signal of Lithium phthalocyanine (LiPc) thanks to the implementation of the automated coupling system. The second part will include a calculation of the relaxation spin states.

9.1 Improved signal intensity

An idea of the implementation of the automated coupling system was very promising. Based on simulations and empirical observations there have been recognized a huge potential for a high gain in signal intensity and resulting signal to noise ratio, which would be beneficial for everybody who runs experiments in Magneto-Optical lab. Before the implementation, the coupling has been done manually. The values in y, z_1, z_2, z_3 were coupled once and then they have not been touched due to extreme time consumption of this procedure. The only value which was used is movement in x direction. After the loading phase, it was roughly coupled manually to some degree of precision. If somebody would like to couple all 5 servo motors at once it would be a task for hours or even days to examine them one by one, hence the fixed positions in 4 directions and a rough coupling in the x.

Presented coupling algorithm couples all 5 servo motors. The time for coupling from the tests was on average twenty minutes. However, the faster coupling process and omitting the necessity of the personal presence is not the greatest benefit, which is the signal to noise ratio gain. The following figure demonstrates the increase in the signal sensitivity. *Before* signal quality was recorded after the manual coupling in x axis with the values of y, z_1, z_2, z_3 used for the majority of the time in the past. *After* values are recorded after the usage of the automated coupling.
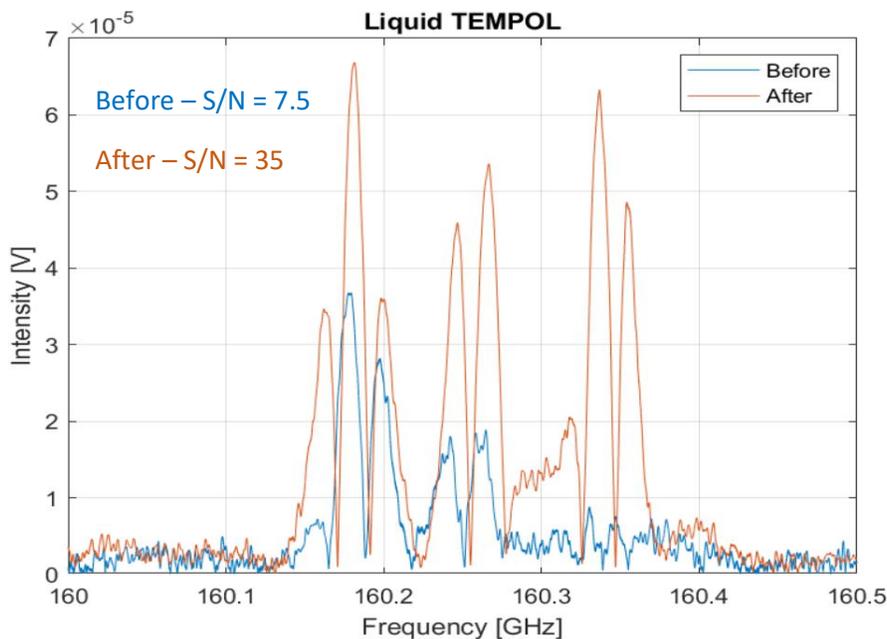
Fig. 8.1   Recorded spectra of the liquid TEMPOL before and after applying the automated coupling with values of signal to noise (S/N) ratios

The coupling algorithm was applied also to the rapid scan measurement of the LiPC. In this measurement, the gain in the intensity was also very large.
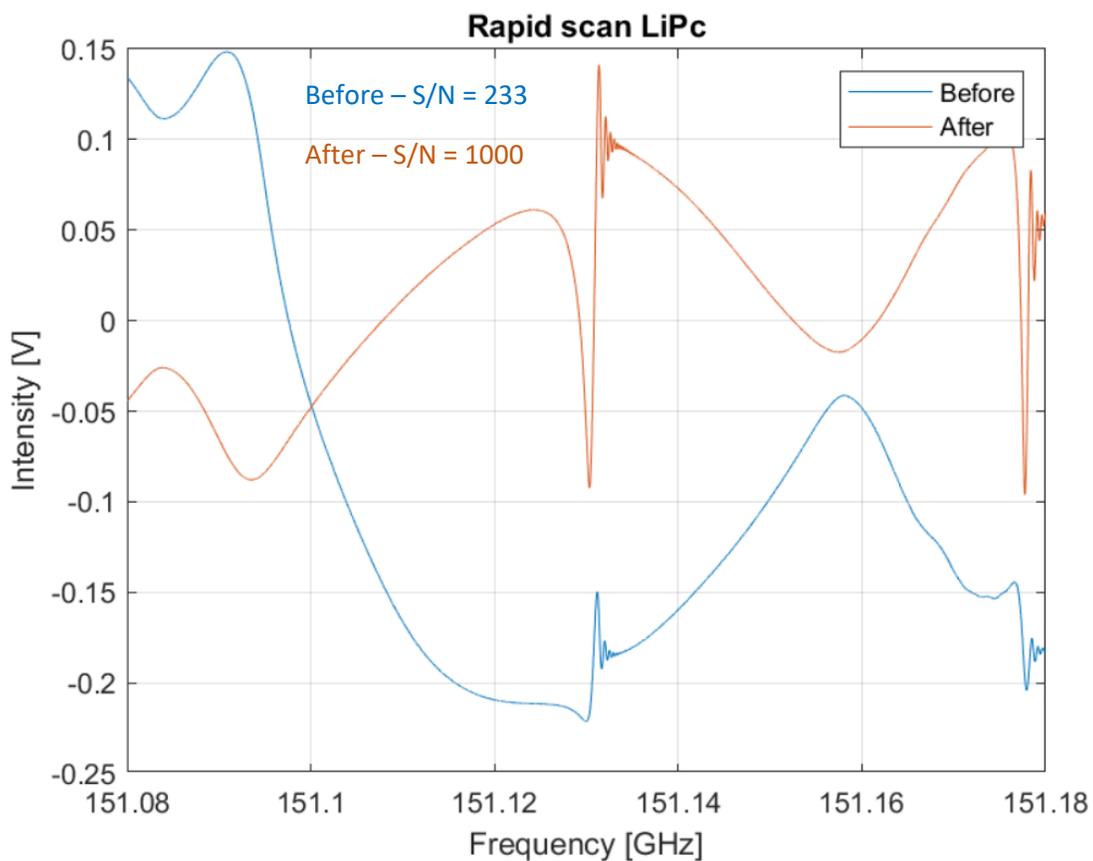
Rapid scan LiPc

Before – S/N = 233

After – S/N = 1000

Intensity [V]

Frequency [GHz]

Fig. 8.2   Recorded spectra of the LiPc by rapid scan method before and after applying the automated coupling with values of signal to noise (S/N) ratios

The value of noise was determined by averaging multiple locations and taking its peak to peak value. The signal quality was also determined by the peak to peak method. These values were divided and this calculation gives the S/N ratio in figures.

9.2 Calculation of the relaxation time

       The calculation is based on the fitting software developed by Dr Oleksii Laguta, which is based on the solving modified Bloch equations. The process of the computation is loading the measured data and then matching simulated curve on top of the measured data. Fig. 8-3A demonstrates incorrectly fitted data (relaxation time is too low, in this case $T_2 = 200\ ns$), Fig. 8-3B represents the correct value of the relaxation time $T_2 = 300\ ns$ with the correct fits of other values of the experiment ($Phase = -18°, Sweep\ shift = 6.3\ MHz, Sweep\ amplitude = 55\ kHz, Sweep\ frequency = 25\ kHz$).
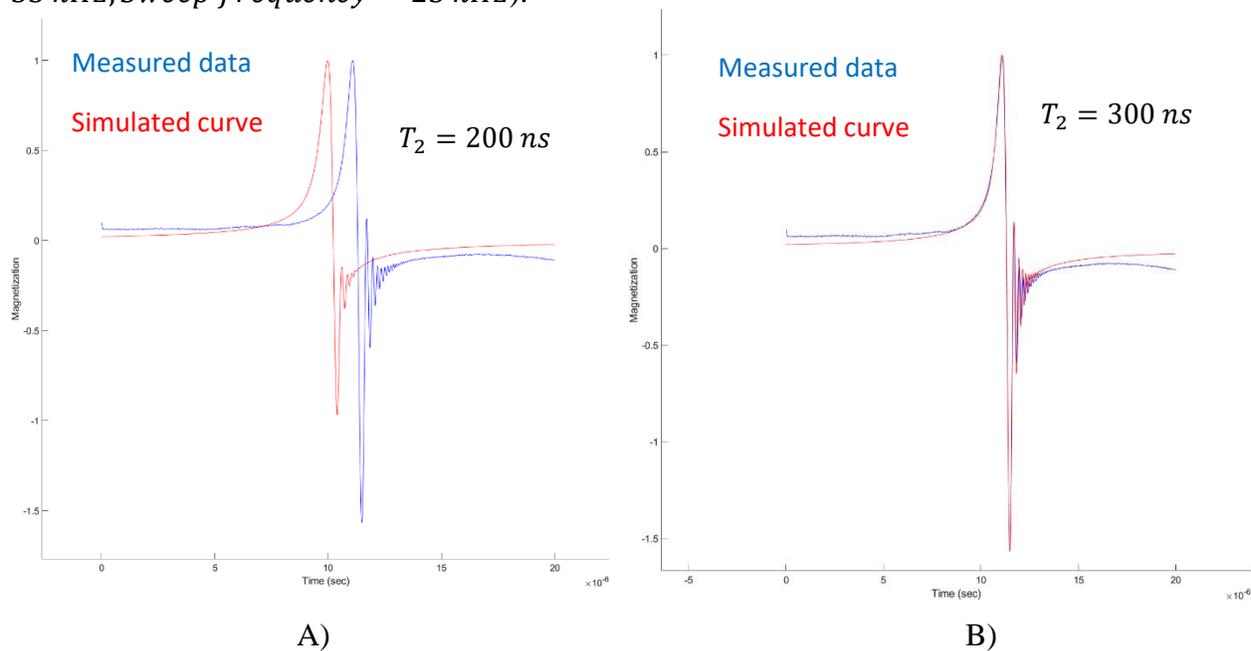
A)   B)

Fig. 8-3   A) Wrong fitting, too low relaxation time. B) Precisefit of parameters of the measurement with resulting relaxation time $T_2 = 300\ ns$

       The final value of the relaxation time from the measured sample of LiPc is $T_2 = 300\ ns$.

10. Discussion

       I would like to discuss several topics from the thesis. The problems I faced, the important notes which surprised me but most importantly the possible enhancement and improvements which may take place after the end of the thesis.

       At first, I would like to talk about the testing holder. It was not the direct goal of the thesis but since I study mechatronics it gave certain mechanical aspect to my work. Although the testing holder was a very tight fit whilst installation, in the end, everything functions and fits perfectly. In the designing process, the virtual model of the spectroscope was used extensively and helped a lot in detailed measurements and final corrections of dimensions of the parts so space would be used to its full potential.

       The majority of the thesis and the majority of the work and time tha was put in was spent on the automatic coupling system. Although, it may seem like a job done, during the process I discovered a lot of flaws, details and huge possible improvements that I would like to continue working on even after the finishing of the thesis. I would like to present a whole new idea of what may be done in the future. There is a working program in the Magneto-optic lab, but I realise that it is not optimal. The design is very simple and it may be considered as a 'student' solution to the problem. The idea, which was consulted with other members of the team, is that the program could be based on a genetic algorithm. I know the limits in which the maximum must occur thus I could get several random starting points at the beginning. I could breed the best of them among each other to get the best place for the signal. I could even introduce random mutations into the process. But this is the melody of the future. I have to admit that I am quite biased to the genetic algorithm and a discussion with the other colleagues will be held before starting this project. I am very curious about their opinions. If the whole idea would be successful, it may potentially be written down and published.

       The implementation of the coupling algorithm had a direct impact on the quality of the rapid scan measurements. This was beneficial for the last task, the calculation of the relaxation times which was set to be $T_2 = 300\ ns$ for LiPc. After recording the spectra, the fitting software was used to fit measured data with the simulated curve.

11. Conclusion

In conclusion, I would like to recapitulate the bullet points of this thesis. The thesis presented the designing process of the automated coupling algorithm and its benefits on the measurements of radicals in HF-EPR spectroscopy.

This work contains the historical introduction to EPR spectroscopy. The theoretical part covers all the essential bits necessary to understand in the field of HF-EPR spectroscopy, coupling of the Gaussian beams and hardware in Magneto-Optical lab at CEITEC BUT.

The practical part covers the mechanical part as a design of the testing holder outside of the magnetic field. The programming part of the automated coupling software demonstrates its impact on the signal to noise ratio in real measurements. The last part is the fusion of the theoretical and practical aspects of the experimental measurement and calculation of the relaxation time with the demonstration of the influence of the implemented software.

The result of this work is currently in use at CEITEC BUT. In the discussion, the idea for future improvements was proposed. If its implementation turns out as a success, the whole idea will be published and shared with other scientific groups around the World.

12. Bibliography

[1] MÖBIUS, Klaus a Anton SAVITSKY. *High-field EPR spectroscopy on proteins and their model systems: characterization of transient paramagnetic states*. Cambridge: Royal Soc. of Chemistry, c2009. ISBN 978-0-85404-368-2

[2] Petr Neugebauer. *Development of Heterodyne High Field / High Frequency Electron Paramagnetic Resonance Spectrometer at 285 GHz*. Physics [physics]. Université Joseph-Fourier - Grenoble I, 2010. English. tel-00454862v5f

[3] DUIN, E. *Short introduction to Electron Paramagnetic Resonance*. Auburn University [online]. Auburn (Alabama): Auburn University College of Sciences and Mathematics, ©2020 [accessed. 2021-05-30]. Available at: http://webhome.auburn.edu/~duinedu/epr/1_theory.pdf

[4] HADDAD, Darine. *Measurement of the Planck constant at the National Institute of Standards and Technology from 2015 to 2017* [online]. 2017 [cit. 2021-5-30]. Dostupné z: https://iopscience.iop.org/article/10.1088/1681-7575/aa7bf2/pdf

[5] GLAESEMANN, Kurt R., Niranjan GOVIND, Sriram KRISHNAMOORTHY a Karol KOWALSKI. EOMCC, MRPT, and TDDFT Studies of Charge Transfer Processes in Mixed-Valence Compounds: Application to the Spiro Molecule †. *The Journal of Physical Chemistry A* [online]. 2010, 114(33), 8764-8771 [cit. 2021-5-31]. ISSN 1089-5639. Dostupné z: doi:10.1021/jp101761d

[6] WEBER, Ralph T. *XENON USER'S GUIDE* [online]. Billerica, MA USA, 2011 [cit. 2021-5-30]. Dostupné z: http://www.nmrcenter.buffalo.edu/EPR_user_guide.pdf

[7] *Table of Fundamental Physical Constants* [online]. [cit. 2021-5-30]. Dostupné z: https://sites.astro.caltech.edu/~george/constants2.html

[8] Electron paramagnetic resonance Zeeman. *ETH Zurich* [online]. [cit. 2021-5-30]. Dostupné z: https://epr.ethz.ch/education/basic-concepts-of-epr/one-elect--in-the-magn--field/zeeman.html

[9] The Spin Hamiltonian. *EasySpin* [online]. [cit. 2021-5-30]. Dostupné z: https://easyspin.org/easyspin/documentation/hamiltonian.html

[10] LEIGH, J.R. Stevenage: Peter Peregrinus, 1988. IEE control engineering series. ISBN 08-634-1111-8

[11] DE SILVA, Akila, Victoria SALEM, Paul M. MATTHEWS a Waljit S. DHILLO. The Use of Functional MRI to Study Appetite Control in the CNS. *Experimental Diabetes Research* [online]. 2012, 2012, 1-13 [cit. 2021-5-30]. ISSN 1687-5214. Dostupné z: doi:10.1155/2012/764017

[12] Dynamic Nuclear Polarization. *Sigmaaldrich* [online]. USA [cit. 2021-5-30]. Dostupné z: https://www.sigmaaldrich.com/technical-documents/articles/stable-isotopes/dynamic-nuclear-polarization.html

[13] Fritzsche, Hellmut and Phillips, Melba. Electromagnetic radiation. *Encyclopedia Britannica*, 23 Jul. 2020, https://www.britannica.com/science/electromagnetic-radiation. Accessed 30 May 2021 Accessed 30 May 2021

[14] Britannica, The Editors of Encyclopaedia. "Poynting vector". Encyclopedia Britannica, 24 Oct. 2016, https://www.britannica.com/science/Poynting-vector. Accessed 30 May 2021

[15] BASSANI, G., Gerald LIEDL a Peter WYDER. *Encyclopedia of Condensed Matter Physics* [online]. Academic Press 2005, 2005 [cit. 2021-5-30]. ISBN 9780122276101. Dostupné z: https://www.elsevier.com/books/T/A/9780123694010

[16] *The Principle of Wave–Particle Duality: An Overview* [online]. Germany, 2010 [cit. 2021-5-30]. Dostupné z: https://application.wiley-vch.de/books/sample/3527412476_c01.pdf

[17] */ Application Notes / Lasers / Gaussian Beam Propagation Gaussian Beam Propagation* [online]. [cit. 2021-5-30]. Dostupné z: https://www.edmundoptics.com/knowledge-center/application-notes/lasers/gaussian-beam-propagation/

[18] GOLDSMITH, P. F. Quasioptical systems: Gaussian beam quasioptical propagation and applications. Piscataway (New Jersey): IEEE Press, [1998]. IEEE Press. ISBN 9780780334397

[19] Distribution of Energy States. *Questions and answers in MRI* [online]. [cit. 2021-5-30]. Dostupné z: http://mriquestions.com/fall-to-lowest-state.html

[20] EasySpin calculator. *EasySpin* [online]. [cit. 2021-5-30]. Dostupné z: https://easyspin.org/easyspin/documentation/tools.html

[21] *CW and Pulse EPR* [online]. [cit. 2021-5-30]. Dostupné z: https://epr.ethz.ch/education/basic-concepts-of-epr/cw-and-pulse-epr.html

[22] BLUME, Richard J. Electron Spin Relaxation Times in Sodium-Ammonia Solutions. *Physical Review* [online]. 1958, 109(6), 1867-1873 [cit. 2021-5-31]. ISSN 0031-899X. Dostupné z: doi:10.1103/PhysRev.109.1867

[23] Eaton SS, Shi Y, Woodcock L, Buchanan LA, McPeak J, Quine RW, Rinard GA, Epel B, Halpern HJ, Eaton GR. *Rapid-scan EPR imaging*. J Magn Reson. 2017 Jul;280:140-148. doi: 10.1016/j.jmr.2017.02.013. PMID: 28579099; PMCID: PMC5523658.

[24] Magneto-Optical and THz Spectroscopy. *SpectroscopyCeitec* [online]. [cit. 2021-5-30]. Dostupné z: http://spectroscopy.ceitec.cz/

[25] BOSMA, H. On Stripline Y-Circulation at UHF. *IEEE Transactions on Microwave Theory and Techniques* [online]. 1964, **12**(1), 61-72 [cit. 2021-5-31]. ISSN 0018-9480. Dostupné z: doi:10.1109/TMTT.1964.1125753 [26] Meyers, R. (2002). *Encyclopedia of physical science and technology*. San Diego, CA: Acad. Press

[27] HESLER, Jeffrey L., LEI LIU, HAIYONG XU, YIWEI DUAN a Robert M. WEIKLE. The development of quasi-optical THz detectors. *2008 33rd International Conference on Infrared,*

Millimeter and Terahertz Waves [online]. IEEE, 2008, 2008, , 1-2 [cit. 2021-5-30]. ISBN 978-1-4244-2119-0. Dostupné z: doi:10.1109/ICIMW.2008.4665521

[28] DEMARTINO, Chris. *Understanding Mixers and Their Parameters* [online]. 2015 [cit. 2021-5-30]. Dostupné z:
https://www.mwrf.com/technologies/components/article/21846332/microwaves-rf-understanding-mixers-and-their-parameters

[29] Lock-in Amplifiers. *Zurich Instruments* [online]. [cit. 2021-5-30]. Dostupné z:
https://www.zhinst.cn/china/cn/lock-in-amplifiers

[30] *What is a Cryostat & How Does It Work?* [online]. [cit. 2021-5-30]. Dostupné z:
https://www.excedr.com/blog/what-is-a-cryostat-how-does-it-work/

[31] *Fundamental Physical Constants* [online]. [cit. 2021-5-30]. Dostupné z:
https://physics.nist.gov/cgi-bin/cuu/Value?hbar

[32] TENNYSON, Jonathan. *Astronomical spectroscopy: an introduction to the atomic and molecular physics of astronomical spectra* [online]. London: Imperial College Press, 2005 [cit. 2021-5-31]. ISBN 18-609-4513-9.

[33] *Proceedings of the National Academy of Sciences* [online]. 13. 1927 [cit. 2021-5-31]. ISSN 0027-8424. Dostupné z: http://www.pnas.org/cgi/doi/10.1073/pnas.13.6.413

[34] Hurst, George Samuel , Graybeal, Jack D. , Stoner, John Oliver and Chu, Steven. "Spectroscopy". *Encyclopedia Britannica*, 29 Mar. 2021,
https://www.britannica.com/science/spectroscopy. Accessed 31 May 2021.

[35] Spin Quantum Number. (2020, August 15). Retrieved May 30, 2021, from
https://chem.libretexts.org/@go/page/2581

[36] E. A. Nanni, A. B. Barnes, R. G. Griffin and R. J. Temkin, "THz Dynamic Nuclear Polarization NMR," in *IEEE Transactions on Terahertz Science and Technology*, vol. 1, no. 1, pp. 145-163, Sept. 2011, doi: 10.1109/TTHZ.2011.2159546.

[37] Rapid Scan EPR. *Bruker* [online]. 2020 [cit. 2021-5-30]. Dostupné z:
https://www.bruker.com/en/products-and-solutions/mr/epr-instruments/rapidscan.html

[38] JAUCH, J. M. a E. L. HILL. On the Problem of Degeneracy in Quantum Mechanics. *Physical Review* [online]. 1940, **57**(7), 641-645 [cit. 2021-5-31]. ISSN 0031-899X. Dostupné z: doi:10.1103/PhysRev.57.641

[39] Hyperfine Splitting. (2020, August 15). Retrieved May 30, 2021, from
https://chem.libretexts.org/@go/page/1795

[40] HECHT, Eugene. *Optics* [online]. 1998 [cit. 2021-5-31]. Dostupné z: doi:978-0-201-83887-9

[41] Interference of Waves. *Physicsclassroom* [online]. [cit. 2021-5-30]. Dostupné z: https://www.physicsclassroom.com/class/waves/Lesson-3/Interference-of-Waves

[42] EAL for LabVIEW by Bosch Rexroth AG. *Vipm* [online]. 2018 [cit. 2021-5-30]. Dostupné z: https://www.vipm.io/package/eal4labview/

[43] ANDRADE, H.A. a S. KOVNER. Software synthesis from dataflow models for G and LabVIEW/sup TM. *Conference Record of Thirty-Second Asilomar Conference on Signals, Systems and Computers (Cat. No.98CH36284)* [online]. IEEE, 1998, , 1705-1709 [cit. 2021-5-31]. ISBN 0-7803-5148-7. Dostupné z: doi:10.1109/ACSSC.1998.751616

[44] BLOCH, F. Nuclear Induction. *Physical Review* [online]. 1946, **70**(7-8), 460-474 [cit. 2021-5-31]. ISSN 0031-899X. Dostupné z: doi:10.1103/PhysRev.70.460

[45] Laguta O, Tuček M, van Slageren J, Neugebauer P. Multi-frequency rapid-scan HFEPR. J Magn Reson. 2018 Nov;296:138-142. doi: 10.1016/j.jmr.2018.09.005. Epub 2018 Sep 19. PMID: 30261338.

13. List of abbreviations, symbols and physical values

Abbreviations

NMR	Nuclear magnetic resonance
EPR	Electron paramagnetic resonance
RADAR	Radio detection and ranging
RS	Rapid scan
CW	Continuous wave
MW	Microwave
MDM	Magnetic dipole moment
VTI	Variable temperature insert
TEMPO	Tetramethylpiperidinoxyl
S/N	Signal to noise
MRI	Magnetic resonance imaging
DNP	Dynamic nuclear polarization
HF-EPR	High field electron paramagnetic resonance

Used physical symbols and constants

n	principal quantum number
l	azimuthal quantum number
m	magnetic quantum number
s	spin quantum number
$\bar{S}$	intrinsic angular momentum spin
$\hbar$	reduced Planck's constant
h	Planck's constant
π	Ludolph number
E	the energy of spin state

ΔE	the energy difference between states
ν	frequency
$\bar{\mu}_e$	magnetic moment of the electron
$\bar{\mu}_n$	magnetic moment of the nucleus
$\bar{\mu}_B$	Bohr magneton
m_s	projection of electron spin
g	Landé factor
B_0	outer magnetic field
H	the spin Hamiltonian
H_{EZ}	Electron-Zeeman Interaction energy
H_{ZF}	Zero-Field interaction energy
H_{NZ}	Nuclear Zeeman interaction energy
H_{NQ}	Nuclear Quadrupole interaction energy
H_{EE}	Electron-Electron interaction energy
H_{HF}	Hyperfine interaction energy
M_o	overall magnetic moment of the system
K_{Long}	Longitudinal coupling coefficient
K_{Lat}	Lateral coupling coefficient
K_{Ang}	Angular coupling coefficient
Δr	Lateral displacement
Δz	Longitudinal displacement
$\Delta \theta$	Angular displacement
M	Magnetic moment
w_0	Beam waist
γ	Electron gyromagnetic ratio
B_1	Microwave magnetic field
P	Power
I	Intensity
N_β	Number of molecules occupying the antiparallel state

N_α	Number of molecules occupying the parallel state
T	Thermodynamic temperature
k	Boltzman constant
c	Speed of light
$\vec{S}$	Poynting vector

14. List of figures

Fig. 8.2   Recorded spectra of the LiPc by rapid scan method before and after applying the automated coupling with values of signal to noise (S/N) ratios

Fig. 8-3   A) Wrong fitting, too low relaxation time. B) Precisefit of parameters of the measurement with resulting relaxation time $T_2 = 300\ ns$

15. List of tables

16. Attachments

External attached files:

A1_Assembly

A2_Plate

A3_BottomHolder

A4_UpperHolder

A5_BottomSlidingBearing

A6_UpperSlidingBearing

A7_Thread

A8_Nut

A9_AutomaticCoupling

A10_SubViInitialPosition

A11_SubViXCouple

A12_SubViYCouple

A13_SubViSigZXYValues

A14_UI